

# NAVAL POSTGRADUATE SCHOOL

## Monterey, California



DTIC QUALITY INSPECTED 4

## THESIS

### DURABILITY MODELING AND DESIGN OF A HELICOPTER ROTOR TIE BAR

by

Gregory P. Sauter

September 1995

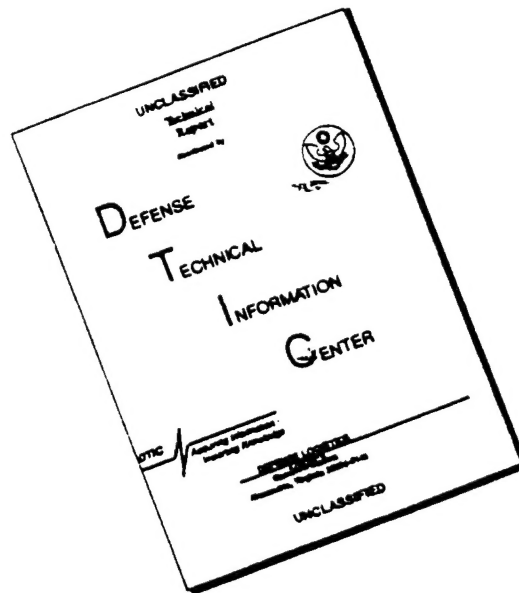
Thesis Advisor:

Edward M. Wu

Approved for public release: distribution is unlimited

19960328 048

# DISCLAIMER NOTICE



THIS DOCUMENT IS BEST QUALITY AVAILABLE. THE COPY FURNISHED TO DTIC CONTAINED A SIGNIFICANT NUMBER OF PAGES WHICH DO NOT REPRODUCE LEGIBLY.

REPORT DOCUMENTATION PAGE			Form Approved OMB No. 0704-0188	
Public reporting burden for this collection of information is estimated to average 1 hour per response, including the time reviewing instructions, searching existing data sources gathering and maintaining the data needed, and completing and reviewing the collection of information. Send comments regarding this burden estimate or any other aspect of this collection of information, including suggestions for reducing this burden to Washington Headquarters Services, Directorate for Information Operations and Reports, 1215 Jefferson Davis Highway, Suite 1204, Arlington, VA 22202-4302, and to the Office of Management and Budget, Paperwork Reduction Project (0704-0188), Washington, DC 20503.				
1. AGENCY USE ONLY (Leave Blank)	2. REPORT DATE September 1995	3. REPORT TYPE AND DATES COVERED Master's Thesis		
4. TITLE AND SUBTITLE DURABILITY MODELING AND DESIGN OF A HELICOPTER ROTOR TIE BAR		5. FUNDING NUMBERS		
6. AUTHOR(S) Sauter, Gregory Paul				
7. PERFORMING ORGANIZATION NAME(S) AND ADDRESS(ES) Naval Postgraduate School Monterey, CA 93943-5000		8. PERFORMING ORGANIZATION REPORT NUMBER		
9. SPONSORING/ MONITORING AGENCY NAME(S) AND ADDRESS(ES) NAVAIRSYSCOM Det PMA(F) - 226 Mr. Jon Winchester Cherry Point, N.C. 28533-0026		10. SPONSORING/ MONITORING AGENCY REPORT NUMBER		
11. SUPPLEMENTARY NOTES The views expressed in this thesis are those of the author and do not reflect the official policy or position of the Department of Defense or the United States Government.				
12a. DISTRIBUTION / AVAILABILITY STATEMENT Approved for public release: distribution is unlimited			12b. DISTRIBUTION CODE	
13. ABSTRACT (Maximum 200 words)  The CH-46 Tie Bar is a multiple leaf, stainless steel system that attaches the rotor blade to the rotating hub and carries rotor blade centrifugal force. The Tie Bar twists as the rotor blade feathers and bends slightly as the Pitch Housing bends. Originally designed to last 3,000 hours without any component breakages, the Tie Bar has experienced field failures that have necessitated inspections every 10 flight hours. Traditional fatigue qualification and life methodology have not reconciled the unusually large number of CH-46 Tie Bar component failures. One CH-46 experienced 15, 10, and 6 component failures on the three aft rotor head Tie Bars after only 93 flight hours. One complete Tie Bar (140 components) failed and caused an aircraft crash.  This research developed a probability modeling predictive method that can aid the design of a Tie Bar that will meet desired life and reliability levels. Laboratory coupon tests were interpreted to provide material properties for several manufacturing processes. Finite element analysis of the current Tie Bar design as well as two modified designs was used to determine the Tie Bar stress state for many component failure combinations. The reduced constraint design produced a dramatic stress concentration reduction and may provide large gains in life over the current and elliptical slot designs.				
14. SUBJECT TERMS Fatigue Life, Probabilistic Fatigue Modeling, Rotary Wing			15. NUMBER OF PAGES 81	
			16. PRICE CODE	
17. SECURITY CLASSIFICATION OF REPORT Unclassified	18. SECURITY CLASSIFICATION OF THIS PAGE Unclassified	19. SECURITY CLASSIFICATION OF ABSTRACT Unclassified	20. LIMITATION OF ABSTRACT UL	



Approved for public release; distribution is unlimited

**DURABILITY MODELING AND DESIGN OF A  
HELICOPTER ROTOR TIE BAR**

Gregory P. Sauter  
Lieutenant, United States Navy  
B.S., United States Naval Academy, 1988

Submitted in partial fulfillment of the  
requirements for the degree of

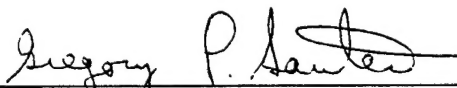
**MASTER OF SCIENCE IN AERONAUTICAL ENGINEERING**

from the

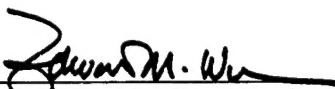
**NAVAL POSTGRADUATE SCHOOL**

September 1995

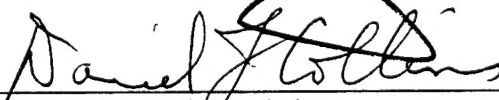
Author:

  
\_\_\_\_\_  
Gregory P. Sauter

Approved by:

  
\_\_\_\_\_  
Edward M. Wu, Thesis Advisor

  
\_\_\_\_\_  
Gerald H. Lindsey, Second Reader

  
\_\_\_\_\_  
Daniel J. Collins, Chairman,  
Department of Aeronautics and Astronautics



## ABSTRACT

The CH-46 Tie Bar is a multiple leaf, stainless steel system that attaches the rotor blade to the rotating hub and carries rotor blade centrifugal force. The Tie Bar twists as the rotor blade feathers and bends slightly as the Pitch Housing bends. Originally designed to last 3,000 hours without any component breakages, the Tie Bar has experienced field failures that have necessitated inspections every 10 flight hours. Traditional fatigue qualification and life methodology have not reconciled the unusually large number of CH-46 Tie Bar component failures. One CH-46 experienced 15, 10, and 6 component failures on the three aft rotor head Tie Bars after only 93 flight hours. One complete Tie Bar (140 components) failed and caused an aircraft crash.

This research developed a probability modeling predictive method that can aid the design of a Tie Bar that will meet desired life and reliability levels. Laboratory coupon tests were interpreted to provide material properties for several manufacturing processes. Finite element analysis of the current Tie Bar design as well as two modified designs was used to determine the Tie Bar stress state for many component failure combinations. The reduced constraint design produced a dramatic stress concentration reduction and may provide large gains in life over the current and elliptical slot designs.





## TABLE OF CONTENTS

I. INTRODUCTION .....	1
A. CH-46 HELICOPTER .....	1
B. PITCH ASSEMBLY .....	2
C. TIE BAR.....	5
D. PROBABILITY MODELING.....	5
II. COMBINATORIAL FAILURE SEQUENCES .....	7
III. FINITE ELEMENT MODELS .....	11
A. CURRENT DESIGN .....	11
B. ELLIPTICAL SLOT DESIGN .....	14
C. REDUCED CONSTRAINT DESIGN .....	14
D. FAILURE STATES .....	16
E. BOUNDARY CONDITIONS .....	17
1. Flight Condition Description.....	18
2. Rotor System Behavior.....	19
3. Conversion of Flight Conditions to Model Boundary Conditions.....	21
IV. FINITE ELEMENT MODEL RESULTS .....	25
V. LIFE PREDICTION .....	37
A. FLAW DISTRIBUTION.....	37
B. COMPONENT LIFE DISTRIBUTION.....	38
C. LIFE CONVOLUTION.....	39
1. Power Law Damage Function.....	40
2. Exponential Law Damage Function .....	42
3. Constant Stress Case Example.....	43
4. Varying Stress Case Based on Rotor Kinematics.....	45
VI. COUPON TESTS .....	47
A. STAMPING FROM NEW DIE.....	47
B. PRE-TWISTING TO 1800 MICRO-STRAIN .....	47
C. 6° TWIST LOAD.....	48
D. DETERMINING MATERIAL PARAMETERS.....	48
VII. CONCLUSIONS.....	57

VIII. RECOMMENDATIONS .....	59
APPENDIX.....	61
LIST OF REFERENCES .....	65
BIBLIOGRAPHY .....	67
INITIAL DISTRIBUTION LIST.....	69

## **ACKNOWLEDGMENTS**

I would like to thank my wife, Karen, and my two children, Calvin and Brooke for their patience and acceptance of my dedication to this work.

I would like to acknowledge the financial support of the Naval Air Systems Command DET, Program Manager Air (Field) - 226.

I would like to thank Professor Gerald Lindsey for his guidance in the development of this work.

Most importantly, I would like to offer my sincerest gratitude to Professor Edward Wu. Through his untiring work ethic, refreshing sense of humor, and true regard for my success, he has shared with me values, knowledge, and a positive attitude which I will value the rest of my life.

## I. INTRODUCTION

### A. CH-46 HELICOPTER

The CH-46 helicopter, pictured below in **Figure I-1** and **Figure I-2**, is operated by both the U.S. Navy and the U.S. Marine Corps. Each rotary wing head on the CH-46 has three rotor blades. A diagram of the rotary wing head is shown in **Figure I-3**. This investigation addresses the analysis and prediction of field failures of the Tie Bars and options for Tie Bar redesign.

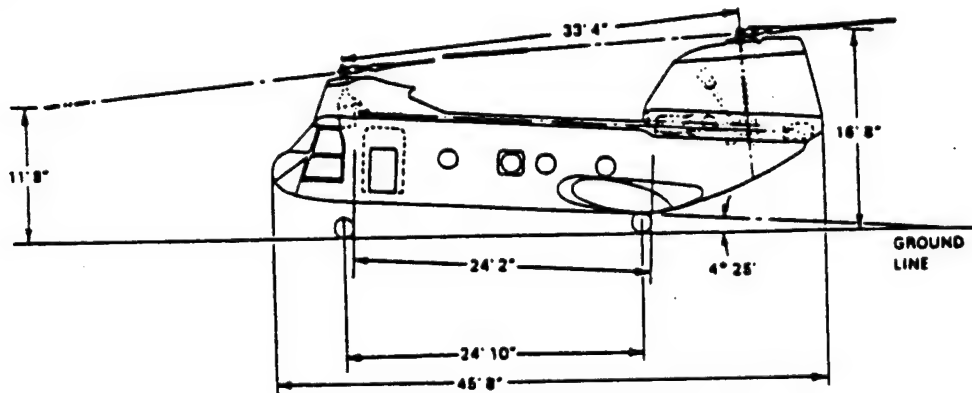


**Figure I-1** CH-46 Helicopter, Side View

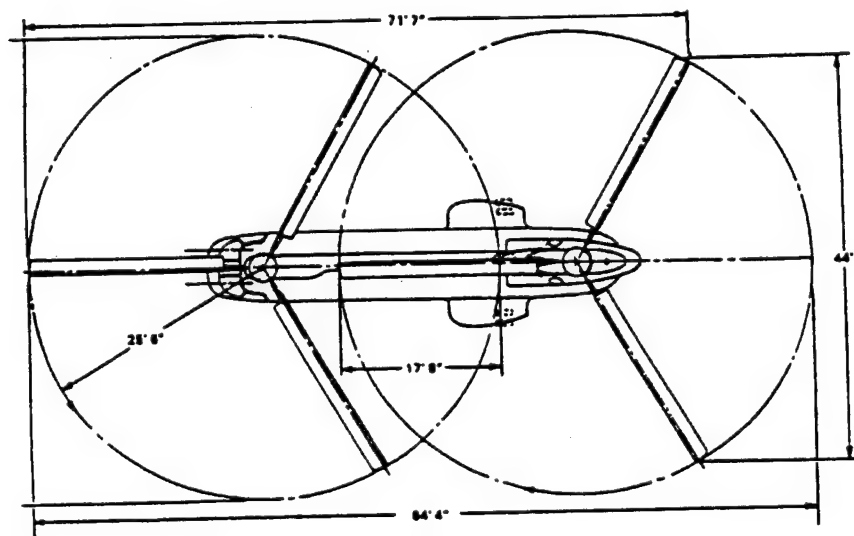


**Figure I-2** CH-46 Helicopter, Top View

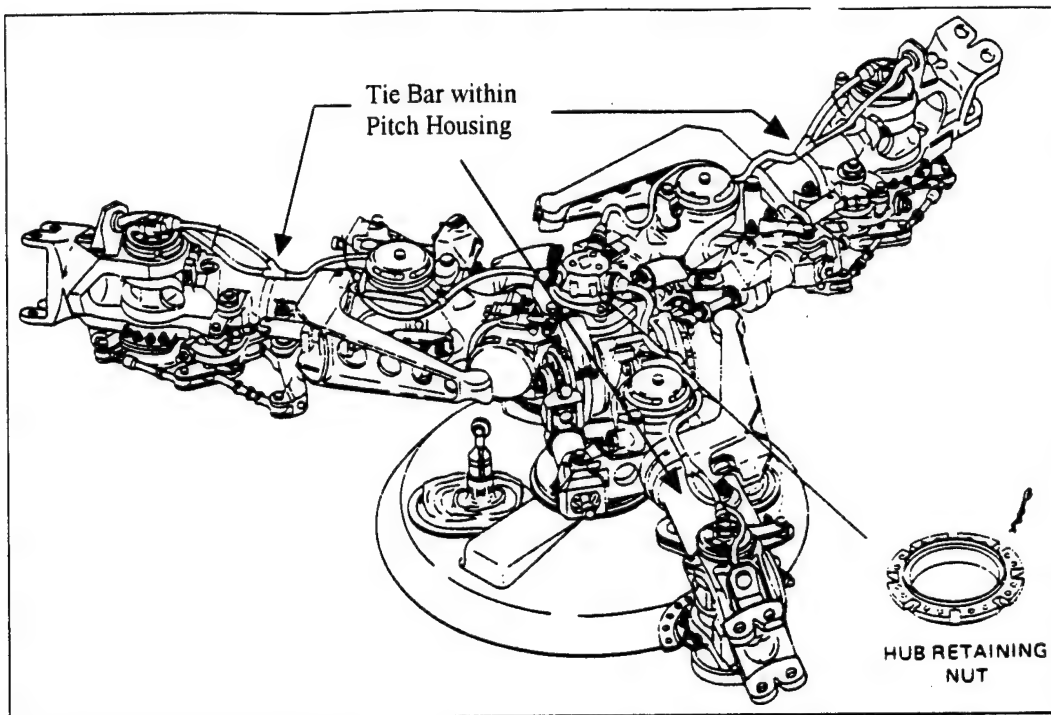


**Figure I-3 CH-46 Rotary Wing Head**

## **B. PITCH ASSEMBLY**

The exploded view of the CH-46 Rotary Wing Head pitch assembly, **Figure I-4**, depicts the Tie Bar and the other rotor blade pitch change components. The cutaway view, **Figure I-5**, illustrates the Tie Bar's location inside the Pitch Housing and Pitch Shaft.

The Tie Bar carries the rotor blade centrifugal force. One end of the Tie Bar is connected to the Pitch Housing; the other end is connected to the Pitch Shaft. There are roller bearings between the pitch shaft and pitch housing that allow relative rotation and sliding between the two parts. Since the Tie Bar is connected to both the Pitch Housing and the Pitch Shaft it twists as control forces are applied to the Pitch Housing to feather the rotor blade. To reduce control loads, the Tie Bar is designed to be soft in torsion. A flatwise bending moment due to flapping applies a bending moment to the pitch shaft and pitch housing which in turn bends the Tie Bar.

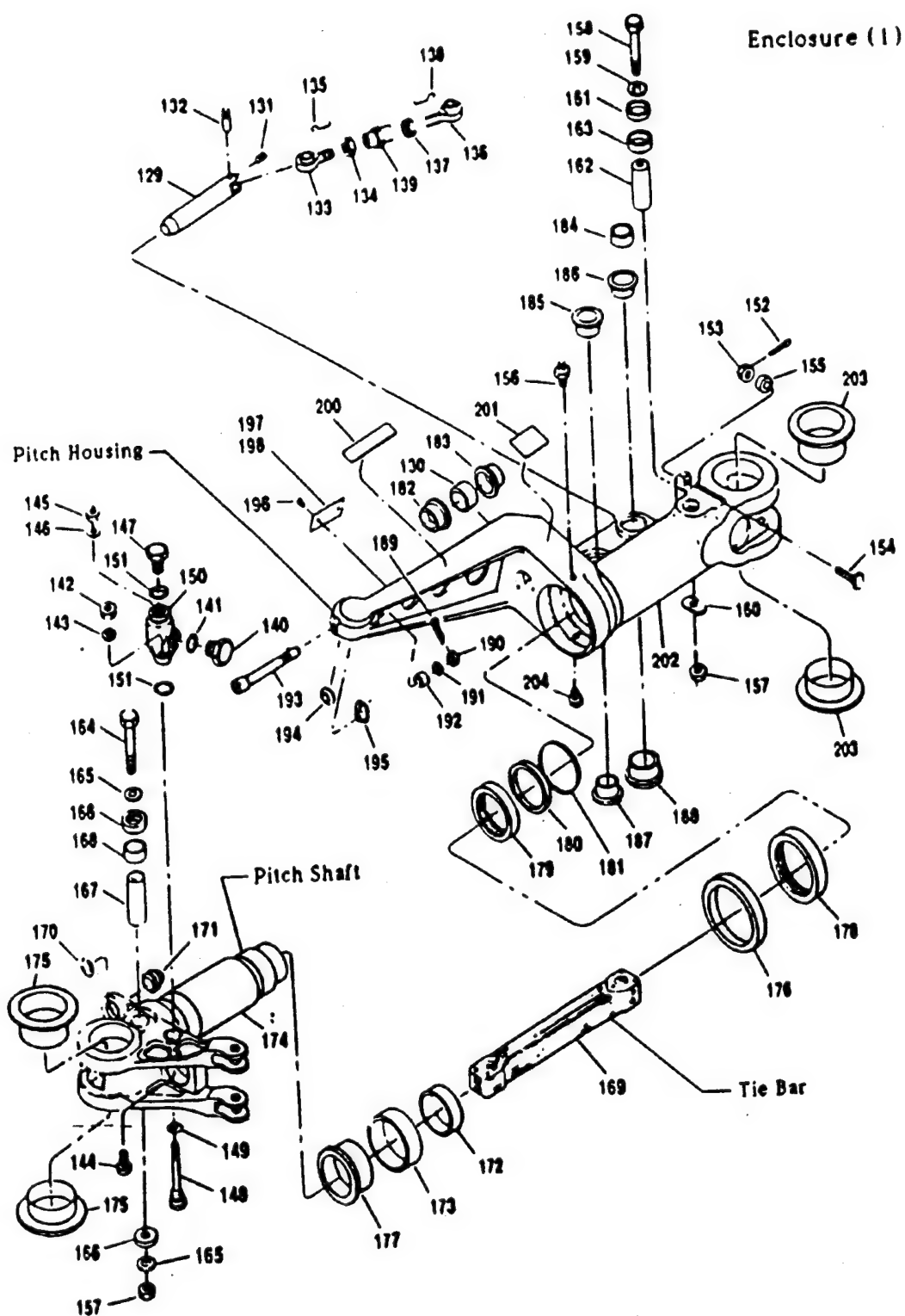


Figure I-4 CH-46 Rotary Wing Head Pitch Change Assembly, Exploded View

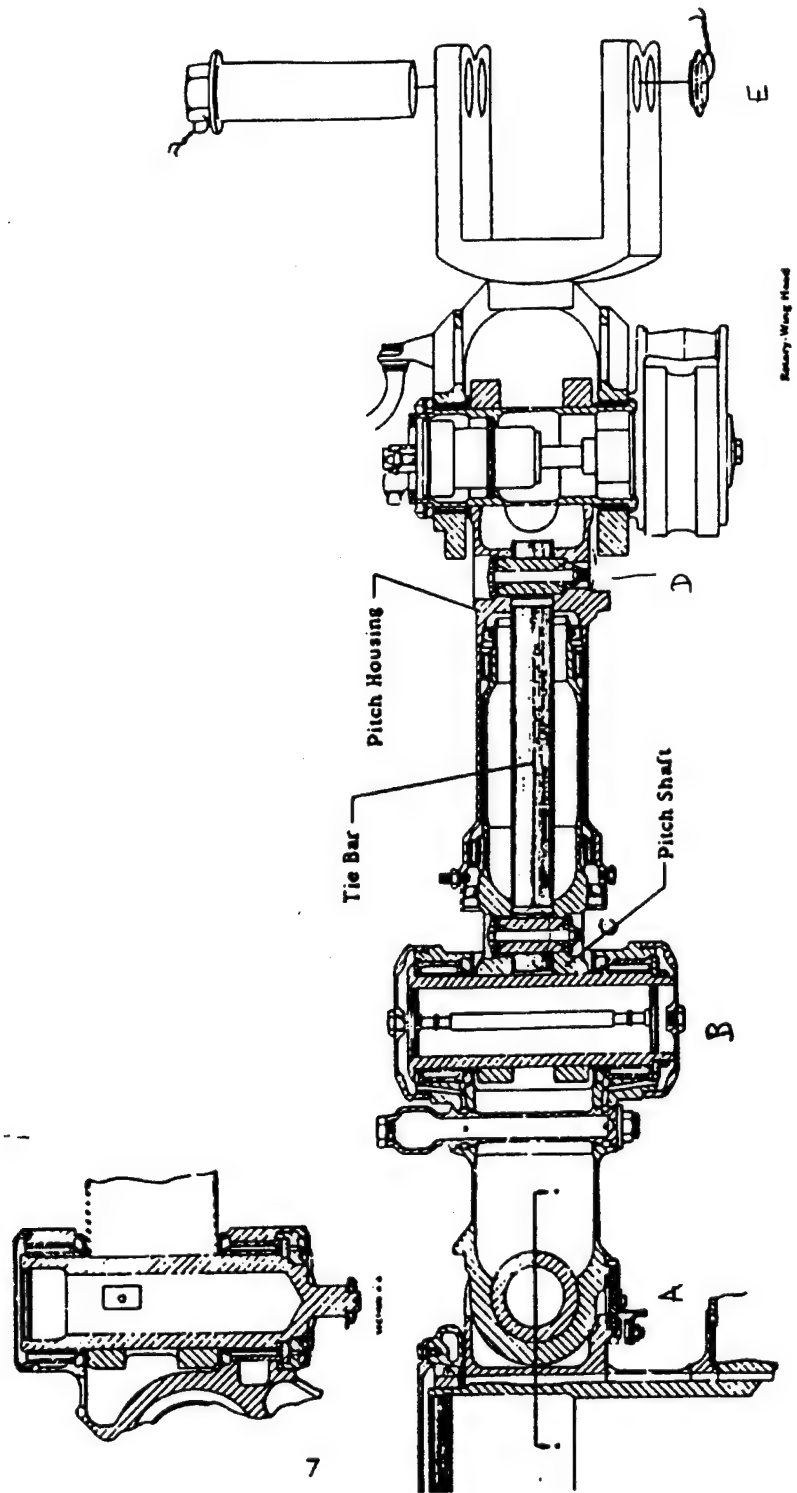
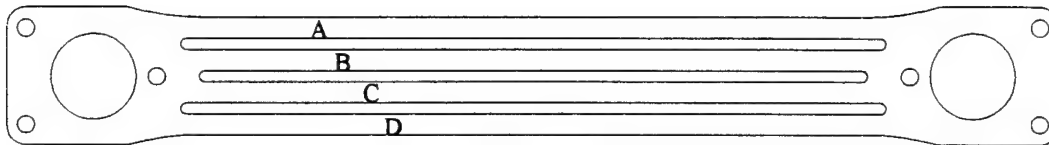


Figure I-5 CH-46 Rotary Wing Head Pitch Change Assembly, Cut-Away View

### C. TIE BAR

The Tie Bar is constructed of 301 Stainless Steel. It consists of 35 slotted straps that are stacked with 301 Stainless Steel spacers in between. The slots, in essence, make each individual Tie Bar strap a redundant four component assembly. The "components" are lettered A through D in **Figure I-6**. The Tie Bar stack is held together by six hollow pins that are expanded by driving a metal ball through them during assembly.



**Figure I-6 Tie Bar Strap Geometry**

Designed to last 3,000 hours without any component breakages, the Tie Bar is now inspected every 10 flight hours. Normal fatigue qualification and life methodology have been unsuccessful in predicting an unusually large number of CH-46 Tie Bar component failures. One CH-46 experienced 15, 10, and 6 component failures on the three aft rotor head Tie Bars after only 93 flight hours. A complete Tie Bar failure has caused one aircraft crash. The cause for early in-service failure of Tie Bar elements has not been determined. Improved manufacturing methods and quality control have not eliminated the problem.

### D. PROBABILITY MODELING

To predict the life of a part by statistics with a high confidence level for safety related components, the number of test specimens must be at least an order of magnitude higher than the desired reliability. For example, to obtain a reliability level of one failed part in 100,000 ( $10^5$ ), at least 1 million ( $10^{5+1}$ ) parts need to be tested. Clearly, this is impractical. In addition, the statistical approach requires building the actual part before the reliability level can be determined. To solve the Tie Bar failure problem, a modeling method needs to be developed that can aid the design of a Tie Bar that will meet desired life and reliability levels.



Since a statistical approach is unrealistic, a probability approach has been chosen. Through a combination of finite element modeling, coupon test analysis, fatigue modeling, and probability modeling, this investigation attempts to develop a model to predict Tie Bar life.

## II. COMBINATORIAL FAILURE SEQUENCES

O'Connor [Ref. 1] studied the Tie Bar problem in a previous investigation. He identified that the probability of failure of a system with multiple components could be determined in terms of the probability of failure of the components. That is, the probability of failure of the Tie Bar can be determined in terms of the probability of failure of the straps which can in turn be determined in terms of the probability of failure *sequences* of the components within the straps. He also identified that each component of a Tie Bar strap can be thought of as a chain in which failure of the weakest link results in failure of that entire component. This lead to adoption of a Weibull distribution for the individual strap components.

$$F(x) = 1 - \exp\left\{-\left(\frac{x}{\beta}\right)^\alpha\right\}.$$

Equation II-1

Applied to the Tie Bar,

$$F_{Ali}[x_A(L)] = 1 - \exp\left\{-\left(\frac{x_A(L)}{\beta}\right)^\alpha\right\},$$

Equation II-2

where  $F_{Ali}[x_A(L)]$  is the probability of failure of component A within a strap under stress  $x_A$  in the  $i^{\text{th}}$  configuration (one, two, three, or four component failures),  $x_A(L)$  is the applied stress on component A caused by the global load  $L$ ,  $\beta$  is a scale parameter of the material strength, and  $\alpha$  is a shape parameter of the material variability. It is important to note that the components have identical failure probability parameters ( $\alpha$ ,  $\beta$ ) because the material is identical, but because the stress states are not the same, each component within a strap has a *different* probability of failure. Finite element analysis is used here to calculate the stress states for input into the probability of failure, Equation II-2. Because of the local stress dependence on the combinatorial failure sequences, the probability of failure of the Tie Bar is no longer Weibull.

A total of 16 failure states exist for a four component Tie Bar strap. Failure states are numbered using a binary code. A 1 represents an unbroken Tie Bar strap component and a 0 represents a broken component. Table II-1 shows the possible failure states and a decimal equivalent name for each failure state.

Component State				Decimal Equivalent
A	B	C	D	
1	1	1	1	15
1	1	1	0	14
1	1	0	1	13
1	1	0	0	12
1	0	1	1	11
1	0	1	0	10
1	0	0	1	9
1	0	0	0	8
0	1	1	1	7
0	1	1	0	6
0	1	0	1	5
0	1	0	0	4
0	0	1	1	3
0	0	1	0	2
0	0	0	1	1
0	0	0	0	0

1 represents an unbroken Tie Bar strap component

0 represents a broken component

**Table II-1 Tie Bar Strap Failure States**

O'Connor [Ref. 1] developed an algorithm to calculate the probability of failure of a Tie Bar leaf given the initial configuration; zero, one, two, three, or four components failed and the final configuration one, two, three, four, or all failed. He first developed an algorithm to calculate a three component system and found that the local stress can be calculated for each break configuration, but the relative strengths cannot be determined unless the failure path which lead to that configuration is known. His three component "failure tree" is shown in Figure II-1.

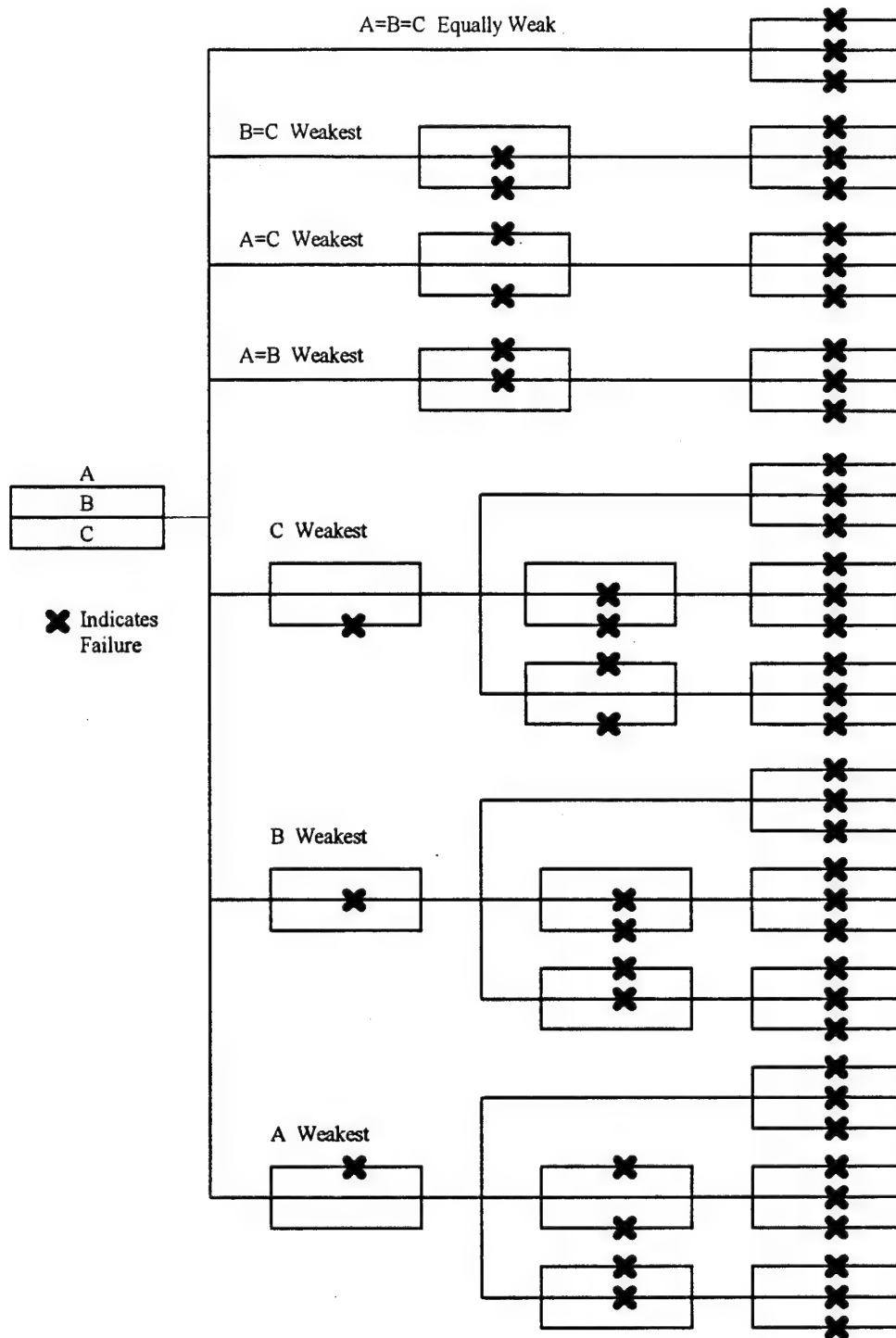


Figure II-1 Three Component Failure Tree

The algorithm to generate the probability of system failure given the component failure first requires calculating the probability of failure of a sequence of consecutive states, (one branch or path of the failure tree). The probability of failure of one sequence is the intersection or product of the transitional probabilities. The probability of failure of the system is the union or sum of the probability of failure of each of the sequences. The appendix of O'Connor's work [Ref. 1] lists all the possible failure permutations for a four component system given that none or any one, two, or three of the four components has already failed.

### **III. FINITE ELEMENT MODELS**

In order to calculate the probability of failure of components of the strap, the stress state at the prospective failure location must be known for each of the physical states, (none failed and partial failures in **Figure II-1**). Finite element analysis is used to calculate such states for three different designs. These designs include:

- A. The current design
- B. An elliptical slot design proposed by Boeing Vertol
- C. A reduced constraint design proposed in this investigation

#### **A. CURRENT DESIGN**

A Finite Element model of the CH-46 Tie Bar, **Figure III-1**, was created using MSC/NASTRAN for Windows. The model consists of the top and bottom straps of the Tie Bar, the three expanded pins at each end of the Tie Bar that hold the assembly together, and the two large pitch housing/pitch shaft pins (parts 162 and 167 of **Figure I-4**) that connect the Tie Bar to the pitch shaft and pitch housing. The straps are modeled using quad PLATE elements. The top and bottom straps are meshed identically.

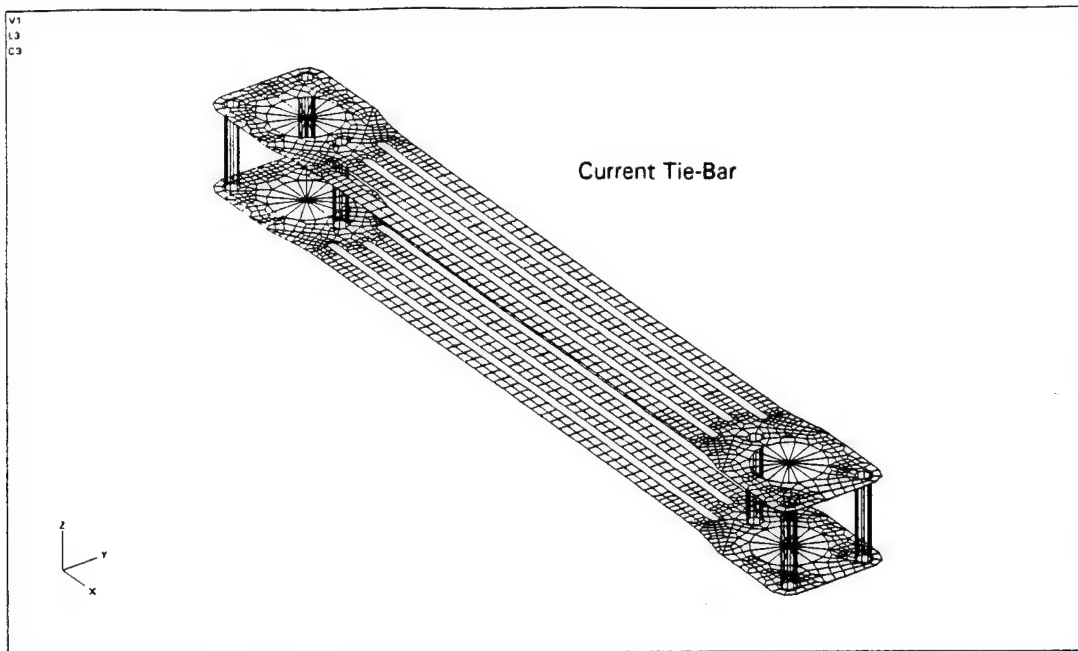


**Figure III-1 Current Tie Bar Finite Element Model**

The expanded assembly pins and pitch housing/pitch shaft pins are modeled using RIGID elements. The assembly pin RIGID elements tie all degrees of freedom of a bottom strap node to a corresponding top strap node. The pitch housing/pitch shaft pins (**Figure III-2**) are modeled by two vertical RIGID elements to which "bicycle spoke" RIGID elements are radially attached. Boundary conditions are applied to the center node of the pitch housing/pitch shaft pins to model the displacements of the Tie Bar in flight.

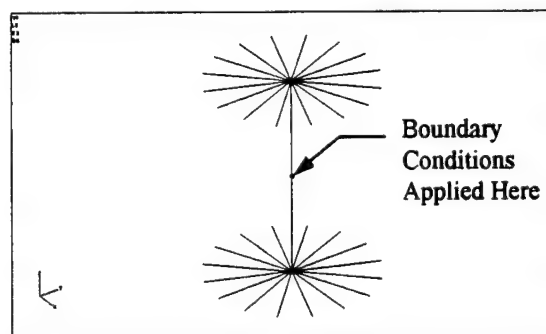


**Figure III-2 Pitch housing/pitch shaft Pin Detail**

The pitch housing/pitch shaft pins in this finite element model are attached to the tie bar straps. These pins in the actual Tie Bar are not attached. Attaching the pins to the Tie Bar straps

provides expedient modeling of the equivalent boundary conditions. The local stress around the pin holes is affected by this expediency; however, service history has shown that failures occur in the 4 components of each Tie Bar strap, not the areas around the holes. Saint-Venant's principle assures that the stresses at actual failure locations, which are far away from the pin holes, are accurately modeled. By applying the boundary conditions to the attached model pins, all the displacement is applied directly to the 4 strap components. The pitch housing/pitch shaft pin holes remain circular; they do not elongate. Therefore, the four strap components experience slightly more strain than the real Tie Bar, and the model is conservative.

The Tie Bar straps are positioned to simulate the maximum allowable Tie Bar stack thickness. The PLATE elements around the pitch housing/pitch shaft pins are thicker than the rest of the Tie Bar. It is assumed that the spacers on both sides of the outermost Tie Bar straps contribute to the strength and stiffness of that region. **Figure III-3** illustrates the thickened region.

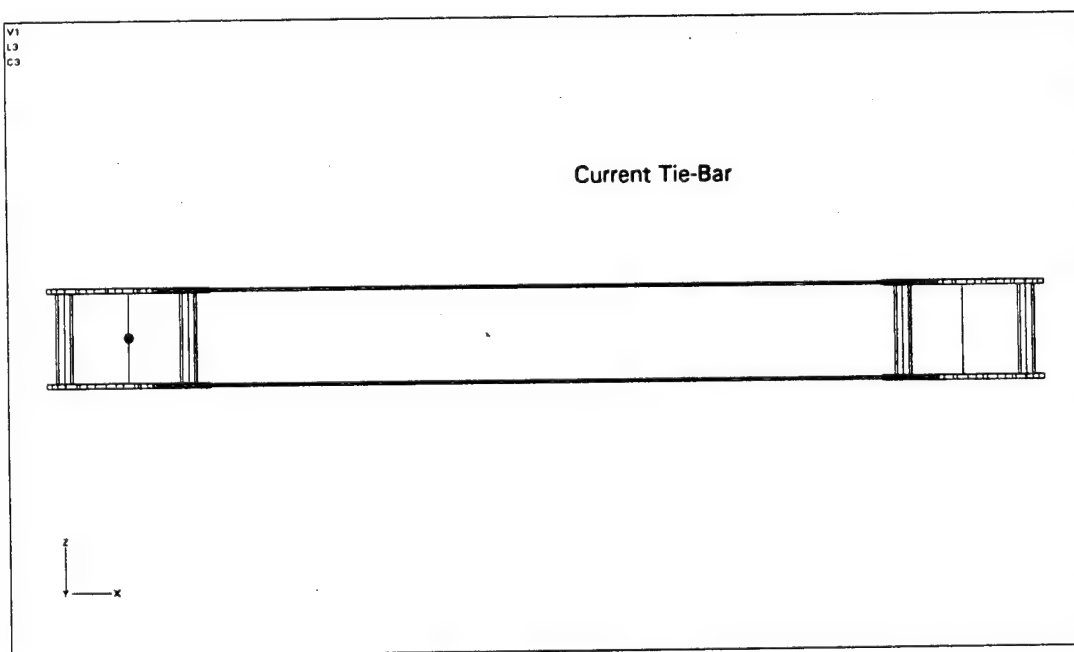


**Figure III-3** Side View of Tie Bar Model Showing Thickened Regions



## B. ELLIPTICAL SLOT DESIGN

The Tie Bar manufacturer, Boeing Vertol, has suggested modifying the geometry of the Tie Bar strap slots to reduce stress concentration and increase Tie Bar life. The focus of the modification is to change the previously semi-circular slot end to a semi-elliptical slot end as shown in **Figure III-4**. This geometric modification was made to the finite element model to replicate the new geometry.

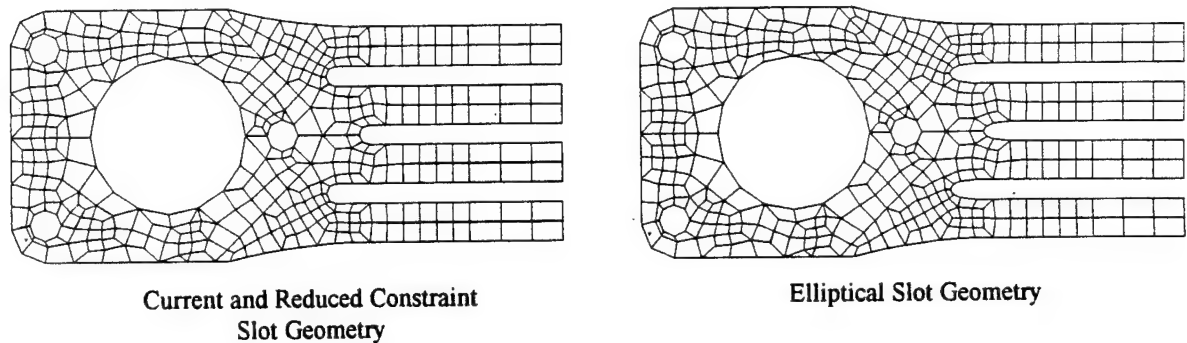


**Figure III-4 Tie Bar Slot Geometry Modification**

## C. REDUCED CONSTRAINT DESIGN

In studying the kinematics of the Tie Bar, it was observed that rotor blade feathering causes straps away from the Tie Bar neutral axis to experience not only a twisting deformation but also a parallel shear. If the three swaged assembly pins around the pitch shaft/pitch housing pins are removed, the reduced constraint significantly minimizes the shear deformation. Without changing the geometry from the current Tie Bar design, another set of models was generated by removing the three swaged assembly pins from each end of the Tie Bar model.

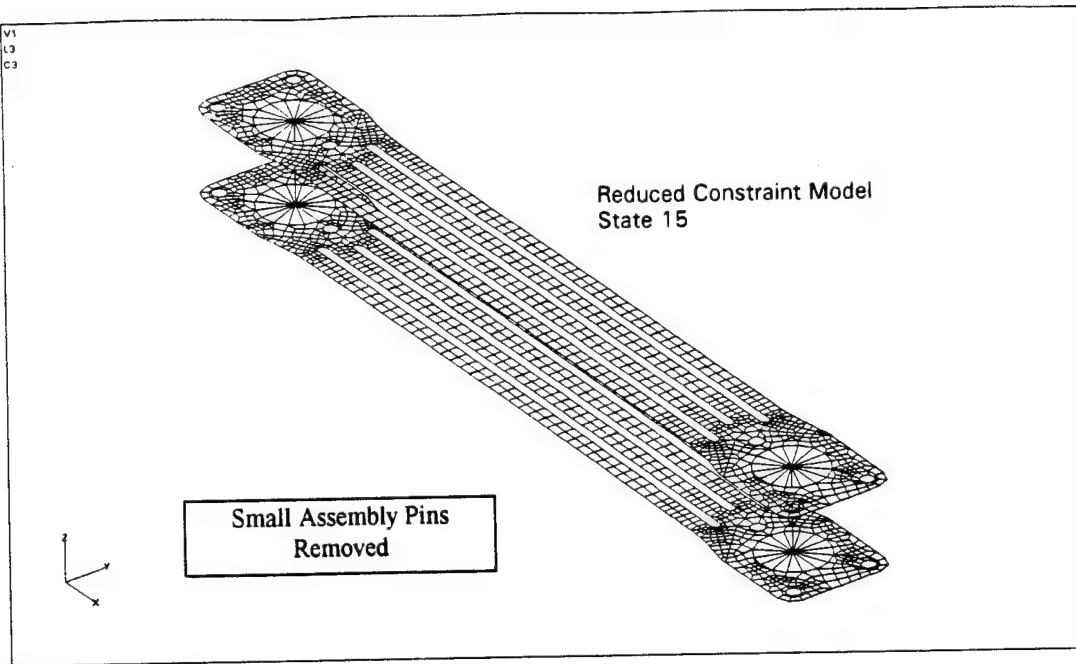


**Figure III-5 Reduced Constraint Tie Bar Finite Element Model**

The straps for the reduced constraint models are only held together by the pitch housing/pitch shaft pin on either end. In a real Tie Bar of this design, the straps could be held together by a sleeve with rolled-over ends, **Figure III-6**. The assembly pin holes would not be required, and the Tie Bar strap ends would be rounded off to maintain clearance inside the pitch

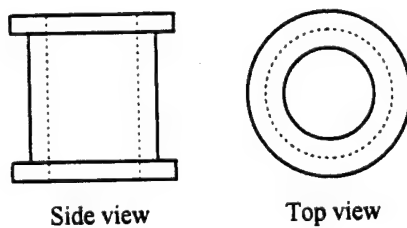


**Figure III-6 Sleeve to Assemble Stack of Reduced Constraint Tie Bar**

shaft when the straps rotate. Also, a low friction material such as Teflon could be used for the spacers between straps to reduce friction. These models were easy to create from the current Tie Bar models and permitted direct comparison.

Whereas the current and elliptical slot design models have all degrees of freedom (DOF) of the pitch housing/pitch shaft pin *end* nodes tied to the pitch housing/pitch shaft pin *master* node,

the reduced constraint model allows the pitch housing/pitch shaft pin *end* nodes to rotate about the pin z-axis relative to the pitch housing/pitch shaft pin *master* node. This design, **Figure III-7**, alleviates in-plane shear and bending of the Tie Bar straps.

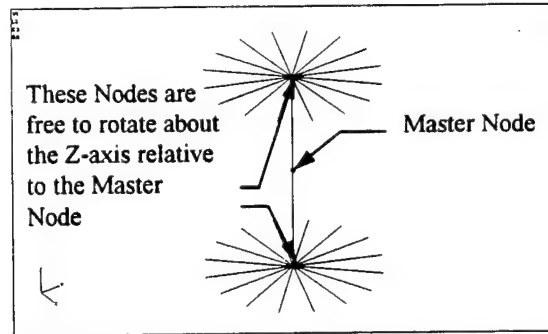


**Figure III-7 Pitch housing/pitch shaft Pin with Rotating Ends**

#### **D. FAILURE STATES**

Models with break sites were created from the unbroken, “parent” models. Individual top strap components were “broken” to simulate breakage in service. This was accomplished by disconnecting the nodes at the prospective failure sites to model the crack trajectory. With the nodes disconnected, the affected PLATE elements in the model were shrunk to show the “break” in the Tie Bar strap.

As stated previously, a total of 16 failure states exists for a four component Tie Bar strap. The possible failure states are shown in **Table II-1**. Six of these states are eliminated using symmetry, and the all-broken state does not require analysis. So, eight models were “grown” from the original model to recreate the possible failure states. **Figure III-8** illustrates a broken Tie Bar model.

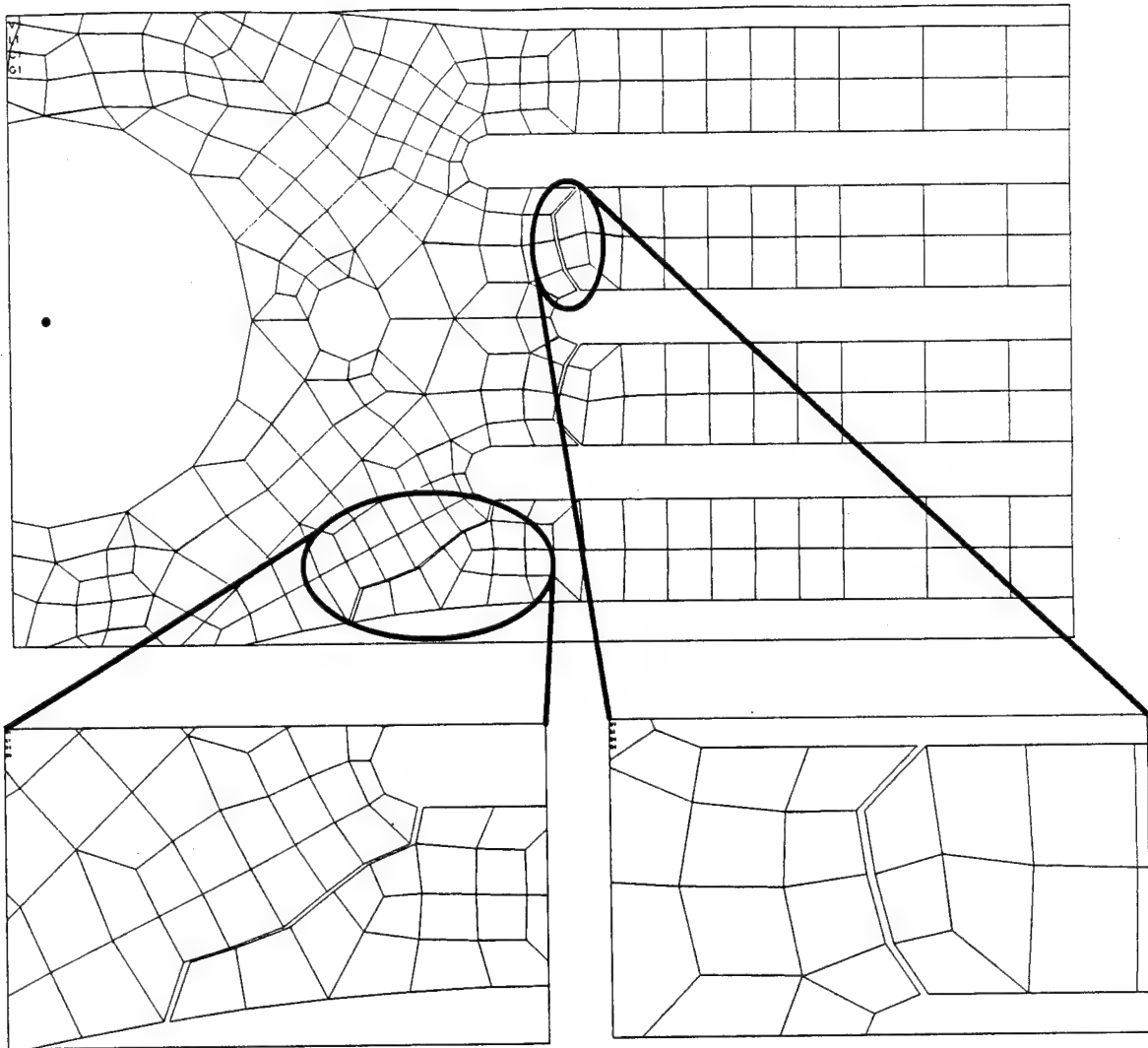


**Figure III-8 Broken Tie Bar Strap**

### **E. BOUNDARY CONDITIONS**

The boundary conditions for the Tie Bar were supplied by the Tie Bar manufacturer as a flight spectrum. For each flight condition, values of centrifugal force, twist, and bending were provided. The flight conditions consist of G-A-G, Pre-Flight, HSLF, Maneuver, and Autorotation, and they are listed with their corresponding Tie Bar displacements in **Table III-1**.

Condition	RPM	CF	Tie Bar Twist♣	Bending♦	Cycles
<u>G-A-G</u>	0→113%→0 0→298 RPM→0	0→76250 lb→0	-25°→-16°→+22°	0→±0.365°→0	1500
<u>G-A-G</u>	0→118%→0 0→312 RPM→0	0→83150 lb→0	-25°→-16°→+22°	0→±0.365°→0	1500
<u>Pre-Flight Maintenance</u>	0	0 0	-25°→+22° ±50°	Negligible 0	6000 5
<u>HSLF</u>	100% Nr 264 RPM	59715 lb	0±6°	±0.23°	3.33×10 <sup>7</sup>
<u>Maneuver</u> 1	105% Nr 277 RPM	65835 lb	5°±7°	±0.275°	9.93×10 <sup>6</sup>
2	105% Nr 277 RPM	65835 lb	5°±8°	±0.275°	36000
3	105% Nr 277 RPM	65835 lb	5°±9°	±0.275°	6000
4	105% Nr 277 RPM	65835 lb	5°±10°	±0.275°	6000
<u>Autorotation</u> 1	113% Nr 298 RPM	76250 lb	-11.6°±4.5°	±0.365°	5.34×10 <sup>6</sup>
2	113% Nr 298 RPM	76250 lb	-10°±6°	±0.365°	0.55×10 <sup>6</sup>
3	113% Nr 298 RPM	76250 lb	-6°±8°	±0.365°	6000
4	113% Nr 298 RPM	76250 lb	-6°±9.4°	±0.365°	3000
5	118% Nr 312 RPM	83150 lb	-11.6°±4.5°	±0.365°	16700
<u>Limit</u>	133% Nr 351 RPM	105630 lb	-20°	0.956°	Once per Lifetime
<u>Ultimate</u>		139960 lb	-20°	1.434°	N/A

♣ Twist cycle is once per rotor revolution for HSLF, Maneuvers, and Autorotation conditions.

♦ Relative angle of attachment pins referenced to the vertical pin. Bending cycle is two times per rotor revolution.

**Table III-1 Tie Bar Loading Conditions**

### 1. Flight Condition Description

The G-A-G condition is a ground-air-ground condition. The first half of the G-A-G cycle includes engaging the aircraft rotors, checking the rotor RPM at maximum throttle with the collective bottomed, and lifting the aircraft off the ground. The second half of the G-A-G cycle includes the aircraft landing and rotor shutdown.

Preflight checks occur on the ground with the rotors disengaged. The collective is moved from full down to full up. The cyclic is moved full forward, full aft, full left, and full right during these checks. These control movements twist the Tie Bar.

HSLF is horizontal steady level flight. It is a cruise condition without climbs, descents, or turns.

Autoration is a power off maneuver in which the collective is lowered and the aircraft's descent is slowed by the windmilling of the rotor blades. As shown in **Table III-2**, autorotation is generally flown at a higher rotor RPM than the other flight conditions.

## **2. Rotor System Behavior**

O'Connor [Ref. 1] conducted a kinematic analysis of a single rotor system in previous Tie Bar research to establish the phasing of the loads and the kinematics of the Tie Bar. A fully articulated system, the CH-46 rotor system has both lead-lag and flapping hinges to provide independent in-plane and out of plane motion of each rotor blade. The rotor blade flapping hinge is designed into the rotor system to prevent development of an undesired rolling moment on the helicopter. Flapping occurs because the advancing rotor blade sees a higher relative velocity and hence higher lift than the retreating blade. Maximum upward flapping occurs at  $\psi = 180^\circ$ , and minimum flapping occurs at  $\psi = 0^\circ$ . Through his research, O'Connor also discovered that the maximum flatwise bending moment occurs at  $\psi = 90^\circ \rightarrow 120^\circ$  (upward) and  $\psi = 270^\circ$  (downward). The rotor angle convention is shown in **Figure III-9**.

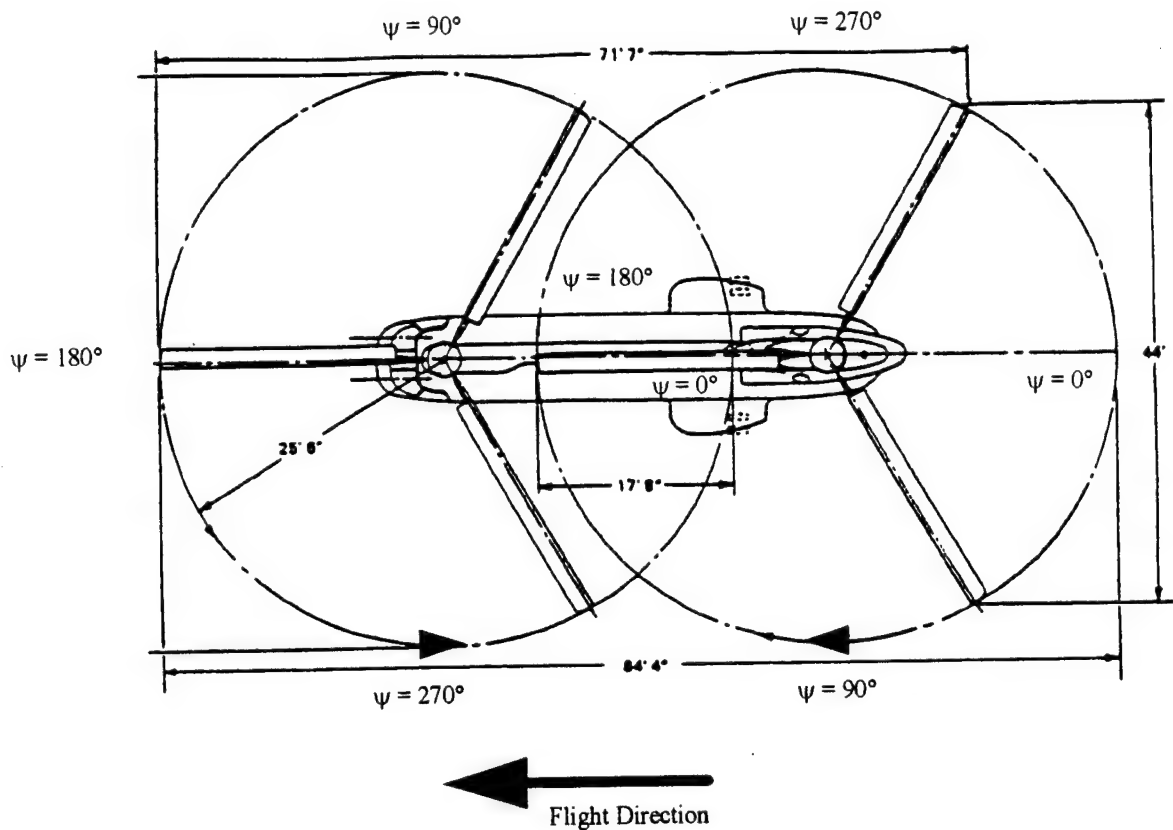


**Figure III-9 Rotor Angle Convention**

Lead-lag is caused by cyclically varying drag and inertia loads. As a blade flaps up, its center of gravity moves inward. Since angular momentum must be conserved, the blade accelerates in plane to compensate for the decrease in moment of inertia. The change in inertia of this upward flapping blade is resisted by the other blades and an in-plane moment is produced. The lead-lag hinge allows the blade to accelerate forward. As the blade flaps down, the center of gravity moves out, and the blade decelerates.

Maximum twist or feathering of the rotor blade occurs at  $\psi = 270^\circ$  where the rotor blade increases pitch to compensate for the lower relative velocity. Minimum feathering occurs at  $\psi = 90^\circ$  where relative velocity is highest.

O'Connor [Ref. 1] also researched the phasing of the Tie Bar bending and twist. He noted that the lead-lag produced negligible bending of the Tie Bar. His study of the rotor blade dynamics produced the results in **Table III-2**.

Rotor Position - $\psi$ (degrees)	Centrifugal Force	Feathering	Bending
0	constant	mean	mean
90	constant	minimum	max up
180	constant	mean	mean
270	constant	maximum	max down

**Table III-2 Rotor Phasing**

### **3. Conversion of Flight Conditions to Model Boundary Conditions**

Three primary load cases were run for each Tie Bar design and break state. The three load cases were:

1. 0.2 inch extension at each pitch housing/pitch shaft pin. (X-translation); **Figure III-10**
2. 0.2 radian twist at each pitch housing/pitch shaft pin. (X-rotation); **Figure III-11**
3. 0.2 radian bending at each pitch housing/pitch shaft pin. (Y-rotation); **Figure III-12**



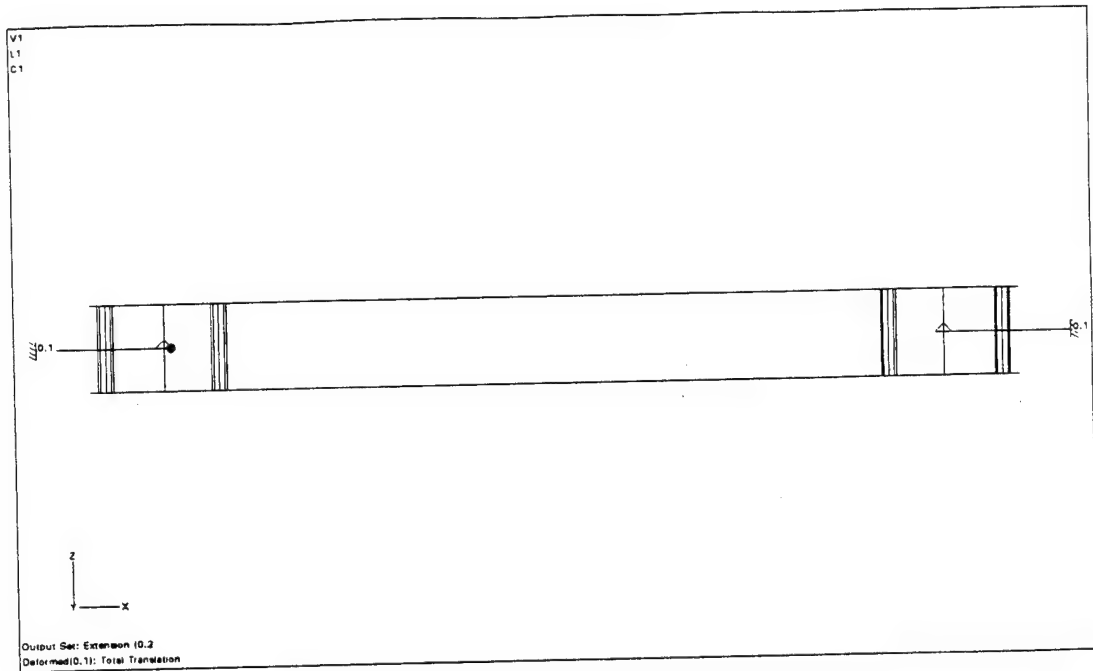


**Figure III-10 Primary Extension Load Case (Side View)**

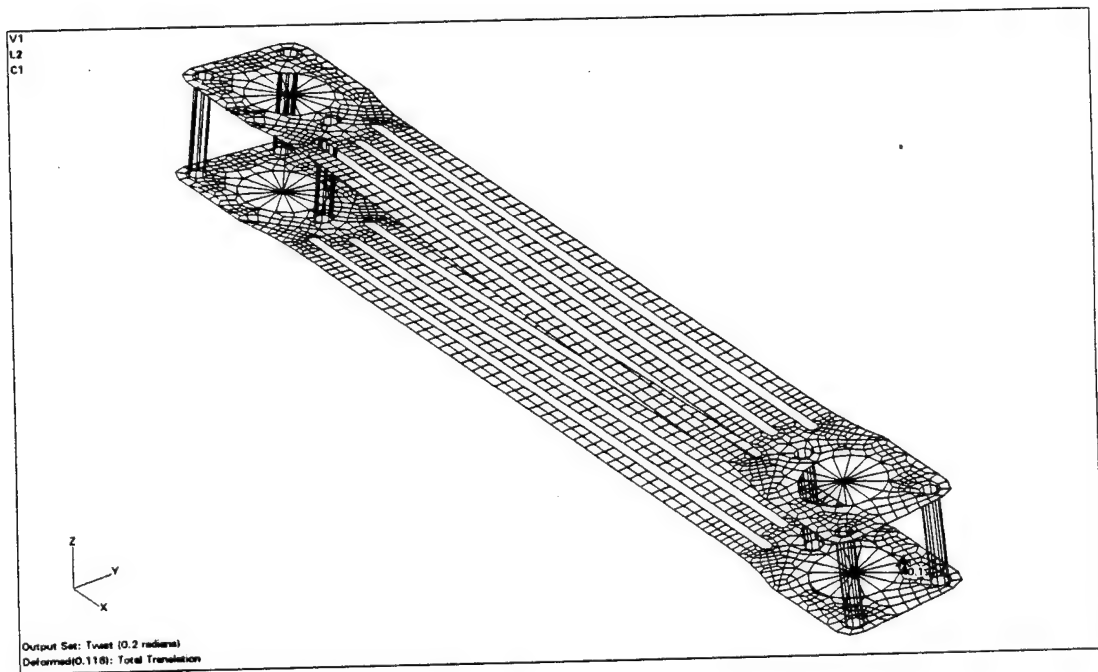


**Figure III-11 Primary Twist Load Case**

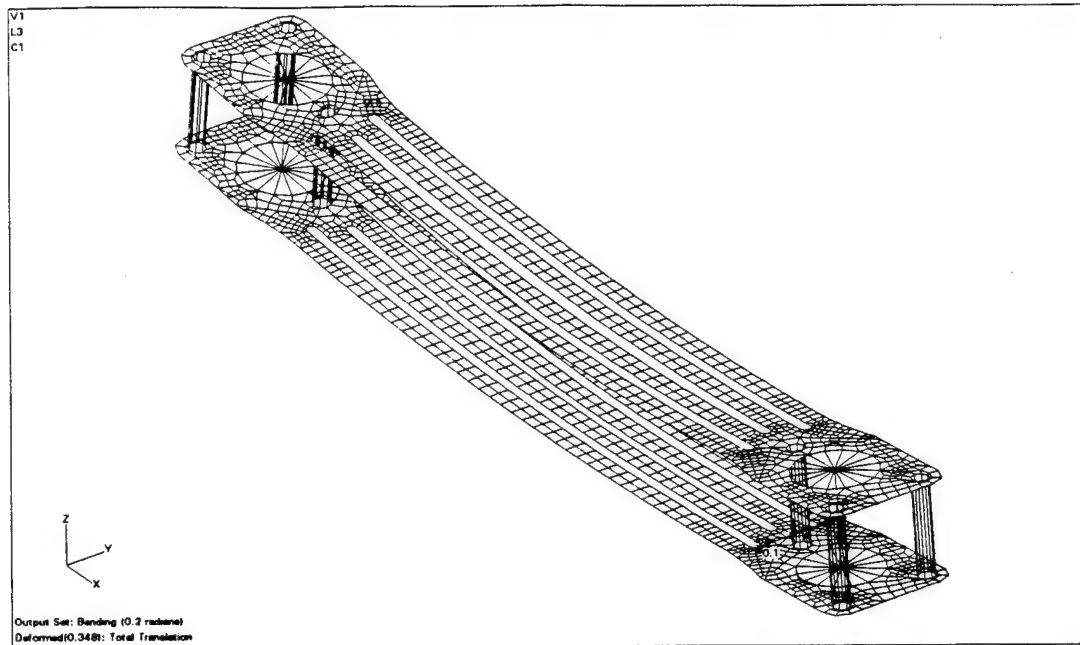


**Figure III-12 Primary Bending Load Case**

These three basic load cases were scaled and linearly combined to recreate each flight condition at  $\psi = 0^\circ, 90^\circ, 180^\circ$ , and  $270^\circ$ . The twist and bending boundary conditions were scaled directly. The extension boundary conditions were given as centrifugal forces instead of displacements. To scale these boundary conditions, the force to extend each unbroken model 0.2 inches was read from the NASTRAN output. This value was divided by 2 to find the force required to deform 1 unbroken strap 0.2 inches. This result was multiplied by 35 to determine the force required to deform a whole 35-strap, unbroken Tie Bar 0.2 inches.

$$(F_{0.2})_{wb} = (F_{0.2})_{2s} \div 2 \times 35,$$

**Equation III-1**

where  $(F_{0.2})_{wb}$  is the force required to deform a whole Tie Bar 0.2 inches, and  $(F_{0.2})_{2s}$  is the force required to deform a two-strap NASTRAN model.

To calculate the extension boundary condition scaling factor the following equation was used:

$$Extension\_scale\_factor = \frac{CF}{\left((F_{0.2})_{2s} - (F_{0.2})_{1s}^u\right) + 34 * (F_{0.2})_{1s}^u},$$

**Equation III-2**

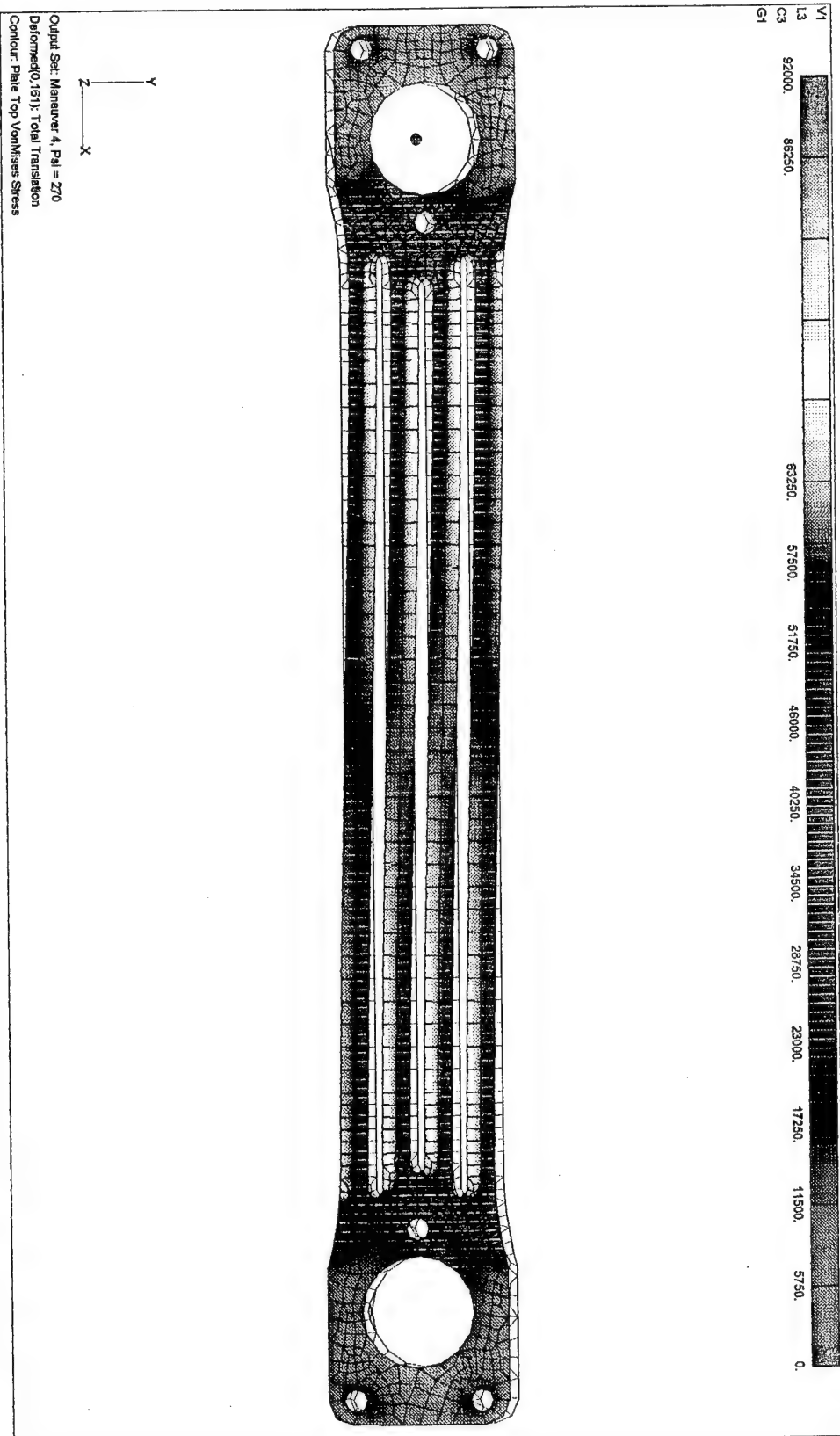
where  $CF$  is the centrifugal force for the given flight condition, and  $(F_{0.2})_{1s}^u$  is the force required to deform one unbroken strap 0.2 inches.

#### IV. FINITE ELEMENT MODEL RESULTS

Service failures of the current Tie-Bar and finite element model stress contour plots indicate that the areas around the Tie-Bar slot ends are most critical. At every spatial location, the 3 scalar components of the stress tensor can be combined to form a scalar value based on the failure process. Since stainless steel is a ductile material, the von Mises failure stress is used. The NASTRAN contour plots that follow, **Figure IV-1**, **Figure IV-2**, and **Figure IV-3** show the deformation and von Mises stress contour of the top strap of the three Tie-Bar designs when the Maneuver 4 flight condition is applied at  $\psi = 270$ . While the Maneuver 4 flight condition at  $\psi = 270$  loads the top Tie Bar strap more heavily than the bottom one, it qualitatively represents typical behavior for the models. The Current Tie Bar and the Elliptical Slot Tie Bar models exhibit in-plane bending caused by the assembly pins. The assembly pins constrain the rotation of the Tie Bar straps about the pitch shaft/pitch housing pins. The Reduced Constraint Tie Bar model exhibits no in-plane bending since the assembly pins have been removed.

The current Tie-Bar model shows areas of high stress where the slots transition from a straight to a radius. The Elliptical Slot Tie-Bar model shows stress concentration in the same areas, but at a slightly lower value. The Reduced Constraint Tie-Bar Model does not show any of the stress concentration of the first two models around the slot ends.

To begin understanding the effect of the new designs on the stress in the Tie-Bar quantitatively, several elements of interest were chosen. These elements are located at the transition between the straight part of the slots and the radiused ends. The element numbers are shown in the "element map", **Figure IV-4**.



(Note shear deformation, left side displaced toward Y+ (up) and right side displaced toward Y- (down)).

Figure IV-1 Current Tie-Bar, Top Strap, Maneuver 4,  $\Psi=270$

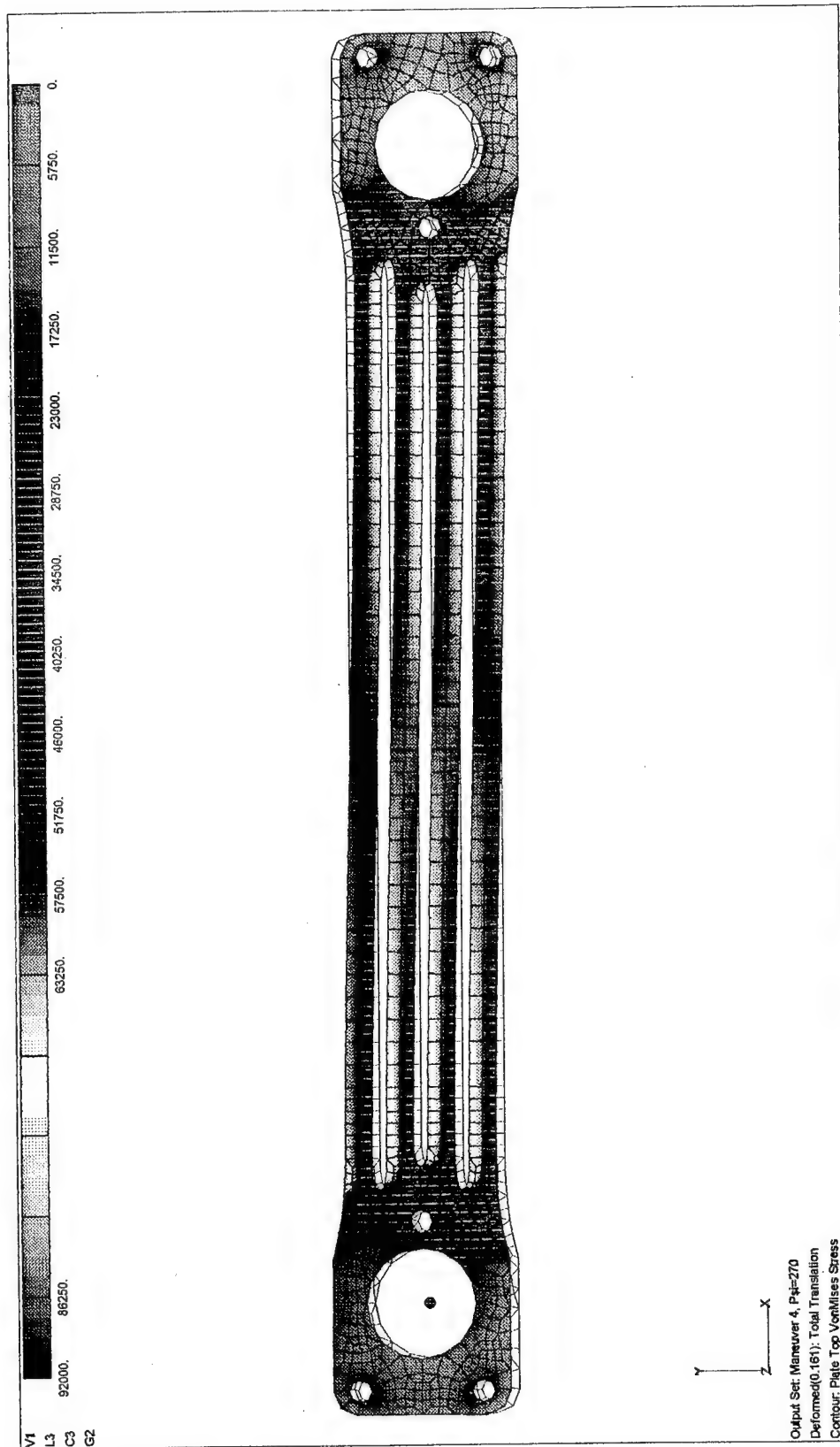
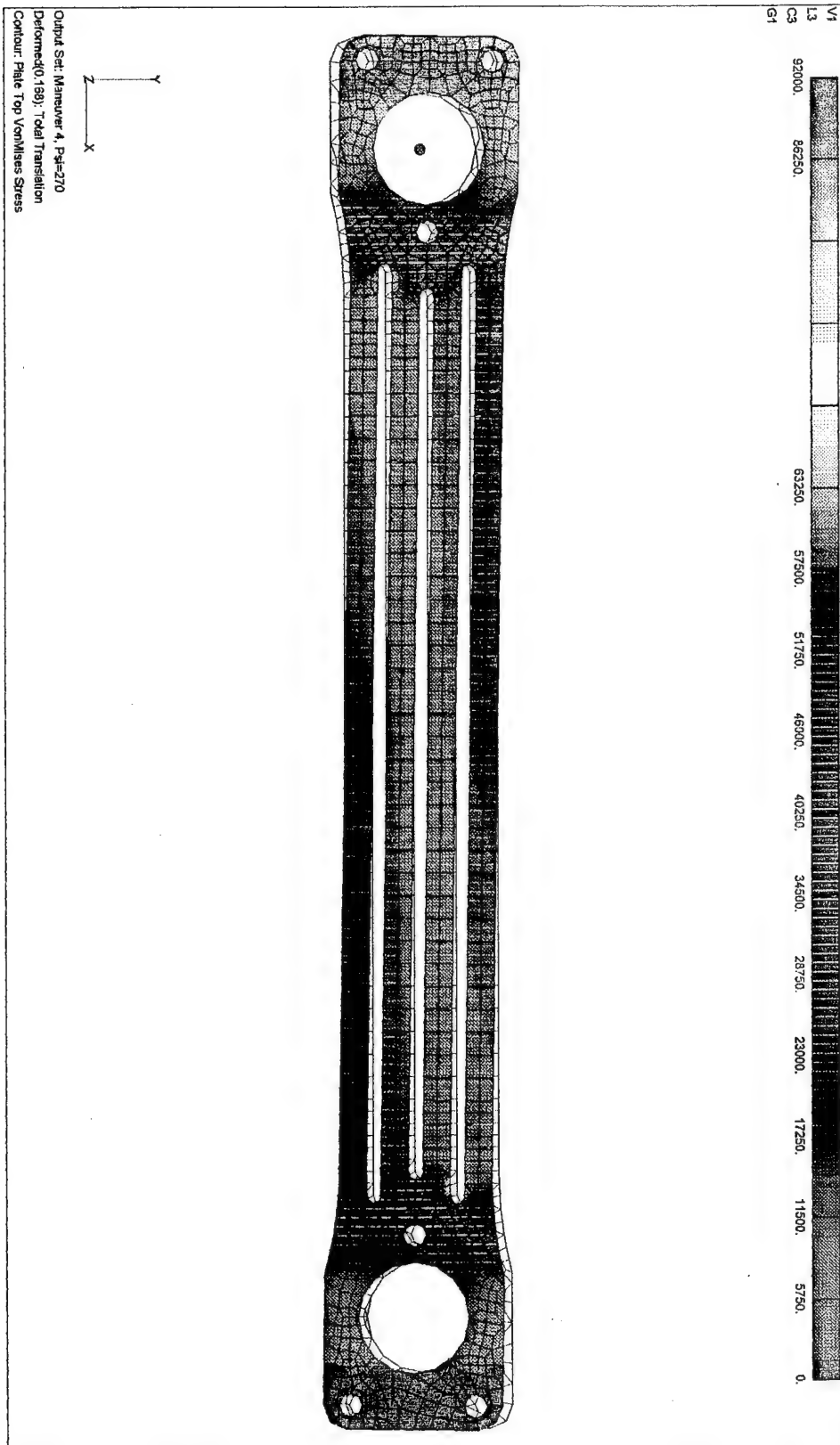
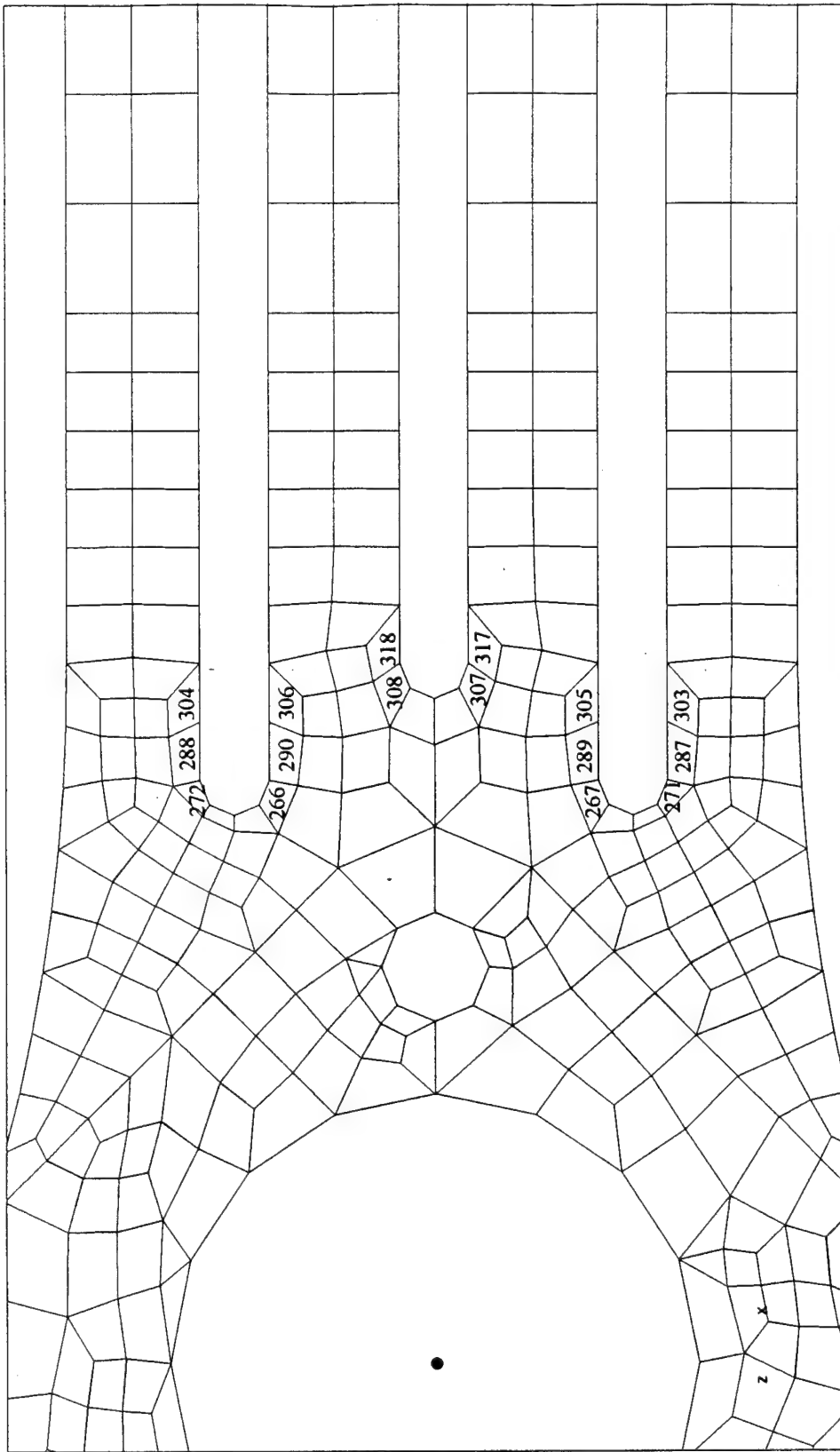


Figure IV-2 Elliptical Slot Tie-Bar, Top Strap, Maneuver 4, Y=270



**Figure IV-3** Reduced Constraint Tie-Bar, Top Strap, Maneuver 4, Y=270



**Figure IV-4 Map of NASTRAN Element Numbers**



Focusing on these “critical elements”, the effect of the design changes was first evaluated by looking at the “critical elements” with the primary load cases applied individually. This allowed study of individual effects on the Tie Bar behavior.

For the extension only load case, the Tie-Bar was elongated 0.02 inches, a typical flight value. When loaded in extension only, the stresses for the Current Tie-Bar and the Reduced Constraint Tie Bar are identical as expected, with the highest values occurring at the inner edges of the outer slots. The maximum stresses for the Elliptical Slot model seem to *shift* away from the slot end slightly. The magnitude is *not* always lower. This suggests that the elliptical slot design may be a benefit to some locations and a detriment to others. Figure IV-5 summarizes these results.

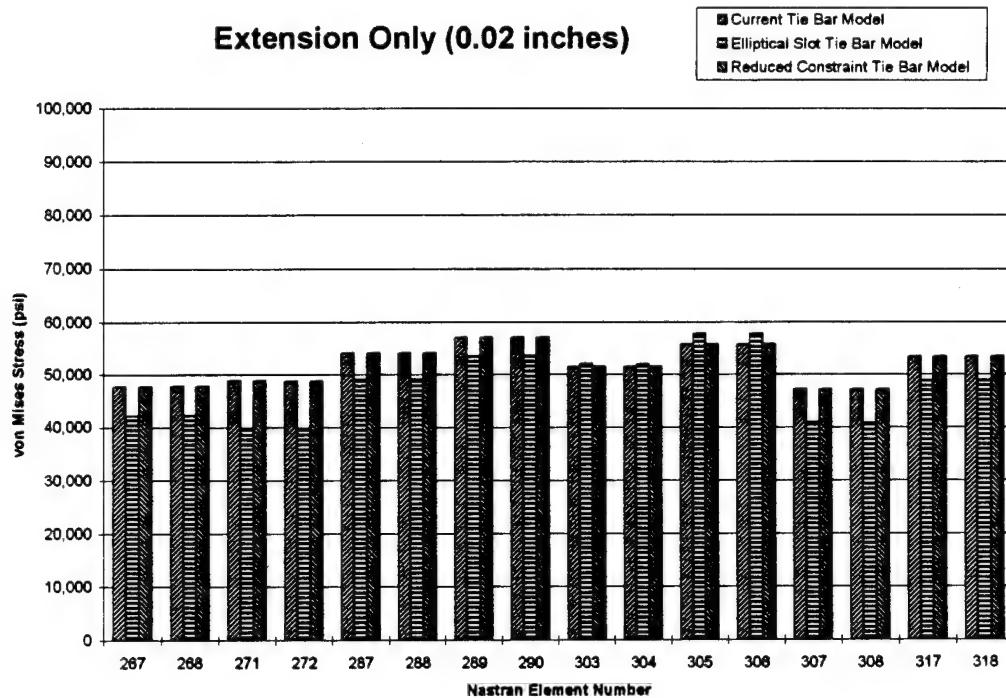


**Figure IV-5 Comparison of Critical Element Stresses for Three Designs, Extension**

In the twist only load case, more dramatic results are evident. Again, the Elliptical Slot model shifts the stress slightly away from the slot end. It also decreases the maximum von Mises stress by nearly 10,000 psi or 17 percent. The Reduced Constraint model shows even more spectacular results. This model reduces the maximum von Mises stress by 31,000 psi or 53

percent. Not only does the Reduced Constraint model drastically reduce the maximum von Mises stress, but it also evens out the stress between the elements. **Figure IV-6** summarizes these results.

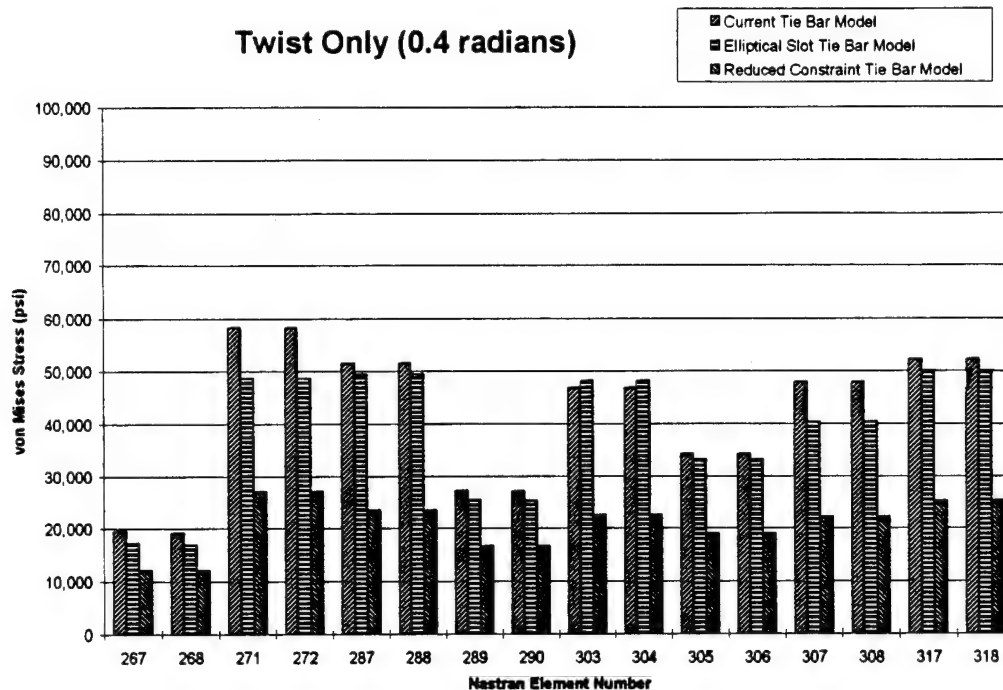


**Figure IV-6 Comparison of Critical Element Stresses for Three Designs, Twist**

The bending only load case causes the models to exhibit behavior similar to that produced by the extension load case. Again, the stress for the Elliptical Slot model moves slightly away from the slot ends. The stresses produced by the bending load case are only about one-fifth those produced by extension and twist. **Figure IV-7** summarizes these results.

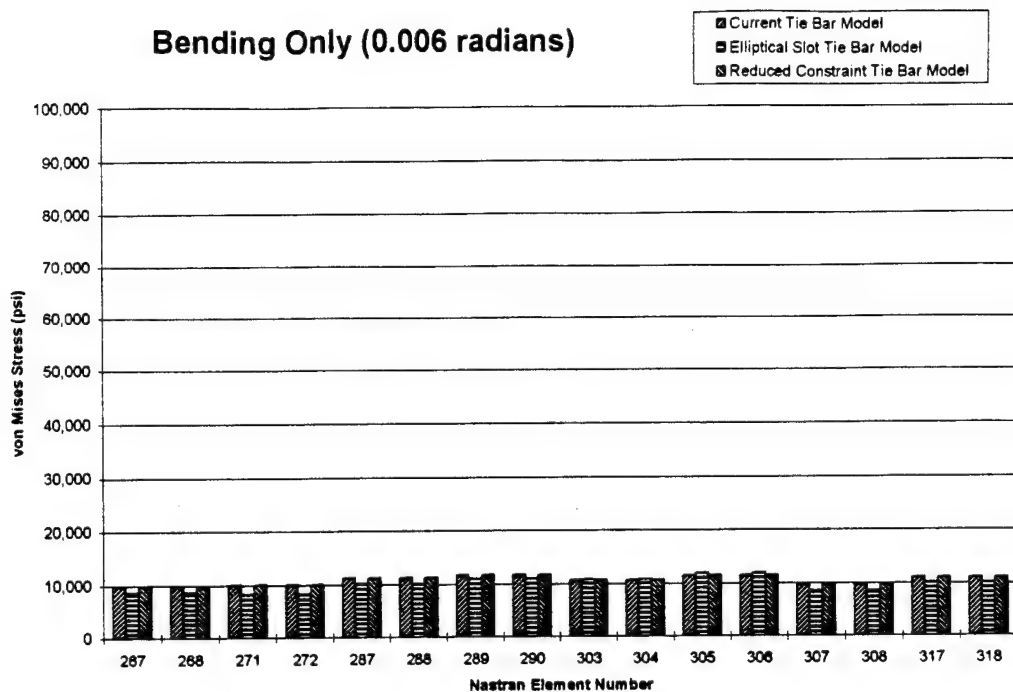


**Figure IV-7 Comparison of Critical Element Stresses for Three Designs, Bending**

To summarize, the stresses due to bending are only one-fifth of those due to extension and twisting. The bending mode is judged to be not critical. Extension induced stresses at all critical locations are within a narrow range. The elliptical slot mainly shifts the maximum stress locations; its benefit is not definitely obvious. The twisting induced stresses are dramatically lowered by 50 percent by the reduced constraint configuration. Serious consideration of this modification is warranted.

Results of the Maneuver 4 flight load case at  $\psi = 270$  are shown in **Figure IV-8**. These results are formed from a scaled linear combination of the above uncoupled load cases. This combined load case indicates that the Elliptical Slot design reduces the maximum stress by about 5,000 psi or 5 percent. The Reduced Constraint design reduces maximum stress by about 25,000 psi or 26 percent. Again it is apparent that the Reduced Constraint design evens out the stresses among the elements. In fact, the Reduced Constraint design shows an *increase* in stress for some elements, but the maximum stress decreases. It is important to remember that these results are for only one flight condition at one rotor position. The trend, however, is significant.

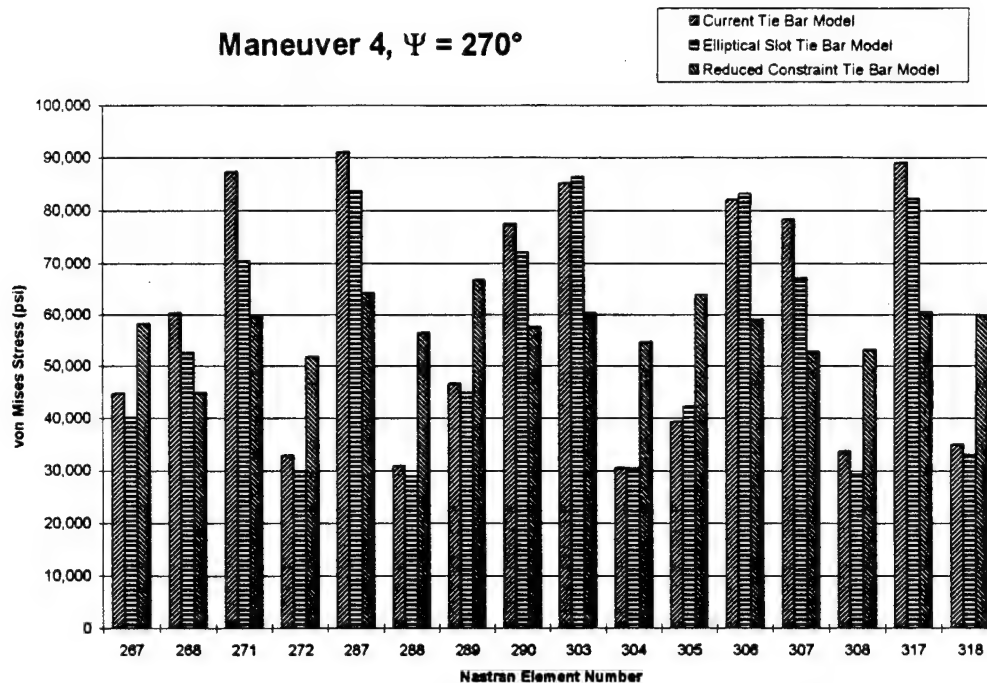


**Figure IV-8 Comparison of Critical Element Stresses for Three Designs, Maneuver 4**

In order to evaluate the cumulative effect of the three designs at the different rotor orientations, results were extracted from the finite element analysis. **Figure IV-9** and **Figure IV-10** show how the von Mises stress varies for one chosen element as the rotor moves through one revolution. The element chosen was the maximum stress element for the flight condition. The solid lines are the current design stresses, the dotted lines are the elliptical slot design stresses, and the dashed lines are the reduced constraint design stresses. The elliptical slot design lowers both the mean stress and stress amplitude slightly. The reduced constraint design lowers both the mean stress and stress amplitude significantly for the Maneuver 4 condition and lowers the mean stress for the  Autorotation 5 condition.

### Maneuver 4

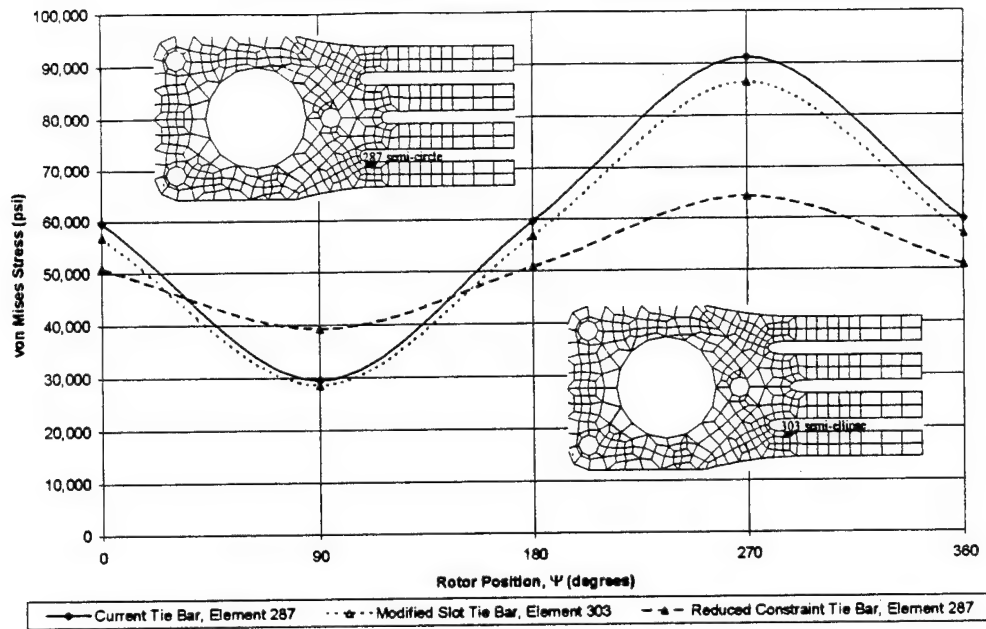


Figure IV-9 Slot End Individual Element von Mises Stresses, Maneuver 4

### Autrotation 5

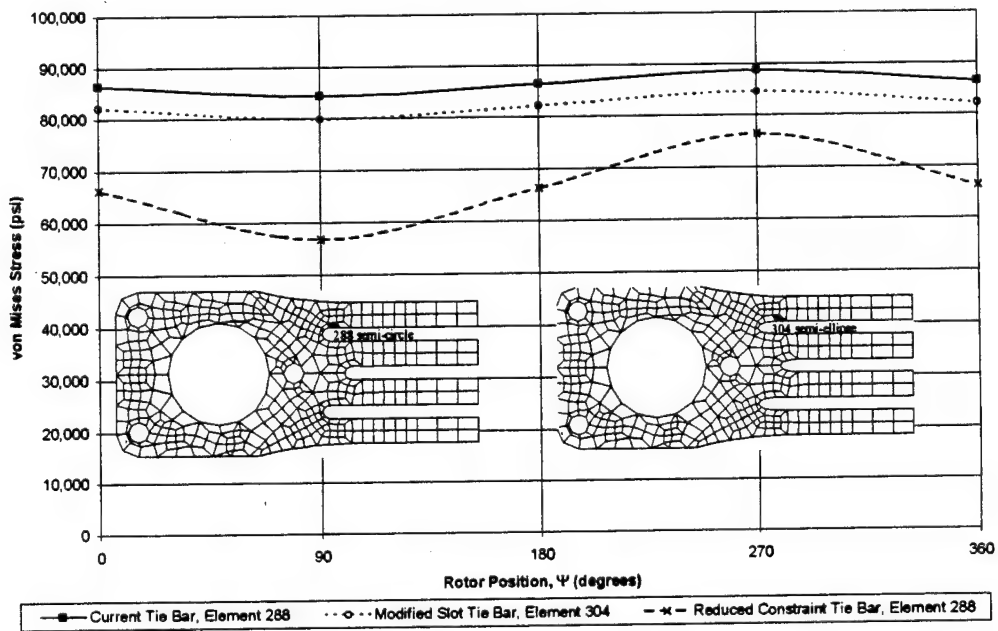


Figure IV-10 Slot End Individual Element von Mises Stresses, Autorotation 5

It is also interesting to note that the moment required to twist the reduced constraint design is significantly lower than that required for both the current and elliptical slot designs. The moment required to twist the modified slot design is greatest. The NASTRAN R1 Constraint Moments for the three designs with a 0.4 radian twist applied are tabulated in **Table IV-1**.

Tie Bar Design	R1 (Twist) Constraint Moment* (in-lb)
Current	43.3
Elliptical Slot	44.0
Reduced Constraint	13.0

\*0.4 radian twist of the two-strap NASTRAN model

**Table IV-1 Tie Bar Constraint Moments**



## V. LIFE PREDICTION

To effectively predict Tie Bar life and evaluate design changes, the probability density function, PDF, and the cumulative distribution function, CDF, for the tie bar system are needed. Determination of the forms of these distributions requires partitioning the Tie Bar system into its components whose distribution functions are known. Conceptually, each Tie Bar strap is first partitioned into 4 components, **Figure I-6**. Each of these components is in turn partitioned into smaller volumes or finite elements. In a finite-element model with all elements of comparable size, any element could describe a metric volume. The size of this metric is arbitrary; a larger metric can be thought of as a combination of smaller metric volumes. A larger metric, however, has a higher probability of failure and a lower strength. The selection of the metric volume is such that the random variable is spatially homogeneous; that is, the stresses are uniformly distributed. The uniform stress criterion is the same as selection for element size in finite element analysis; as a result, the element can be used directly as a metric.

### A. FLAW DISTRIBUTION

The mechanistic bases for failure in metals are by flaw growth and by dislocations. For brittle failure modes, a given element contains flaws that are either smaller than some critical flaw size,  $a < a_c$ , or larger,  $a \geq a_c$ . Each element can be considered flawed or not flawed based on this criterion. In other words, scanning each element for flaw size would create two categories of elements, those with flaw sizes greater than or equal to critical, and those with flaw sizes less than critical. There are only two possibilities for each element, pass or fail. Respective to the critical flaw size, the exceedences are binomially distributed. The binomial distribution has the form:

$$f(n) = C_n^N p^n (1-p)^{N-n},$$

Equation V-1

where  $f(n)$  is the probability density function, pdf,



$$C_n^N = \frac{N!}{(N-n)!n!},$$

Equation V-2

$p$  is the probability that the element has  $a \geq a_c$ ,  $n$  is the number of elements that have  $a \geq a_c$ , and  $N$  is the total number of metric elements being considered. In the current investigation, it is the total number of elements in each strap.

When the number of elements is large, and the flaw density is low, then the probability density function, pdf, takes on the Poisson distribution form:

$$f(n) = \frac{\mu^n}{n!} e^{-\mu},$$

Equation V-3

where  $\mu = Np$  and is assumed to remain constant.

For fatigue, the location parameter of the distribution of flaws is time dependent. As time increases, flaws grow and the probability that flaws exceed the critical size increases. The binomial distribution then, is a snapshot in time.

## B. COMPONENT LIFE DISTRIBUTION

For any given instant in time, in order for a given component to have life  $\tau$ , each of its elements must have life  $\tau$ . In other words, element 1 and element 2 and element 3 and ... element  $n$  must have life  $\tau$  in order that the entire system has life  $\tau$ . Conversely, if any one element does not have life  $\tau$ , the whole component fails. In other words, when the weakest-link fails, the system fails. In terms of the previous discussion, when any element experiences crack growth to a size greater than the critical dimension, the whole Tie Bar component fails.

In Boolean algebra, the weakest link system reliability is the intersection ( $\cap$ ). The reliability of the components is conceptually a chain, or *series*, of links with no *parallel* or redundant links. For a three component system where  $R$  denotes reliability or probability of non-failure,

$$R_3\{X_1 \cap X_2 \cap X_3\} = R\{X_1|X_2 \cap X_3\}R\{X_2|X_3\}P\{X_3\}.$$

Equation V-4

Assuming now that the component is made up of many elements and the reliability of each is independent,

$$R_n = R\{X_1 \cap X_2 \cap X_3 \cap \dots \cap X_n\} = R\{X_1\}R\{X_2\}R\{X_3\} \dots R\{X_n\},$$

Equation V-5

where  $R_n$  denotes the Tie Bar component reliability. In this case, the component being discussed is itself a system of elements or links in the chain. Failure is assumed homogeneous to mechanism. In other words, failure is not related to the size of a component. A larger component will have more elements, but the flaw *distribution* does not change. When this is true, a hazard function  $\Xi(\tau)$  is defined which takes on the Weibull form,

$$\Xi(\tau) \equiv \tau^a,$$

Equation V-6

where  $\Xi(\tau)$  is the system reliability or hazard function,  $\tau$  is the life of a single element, and  $a$  is the number of elements in the component. The cumulative distribution function, CDF, can then be written as:

$$F(t) = 1 - \exp[-\Xi(\tau)].$$

Equation V-7

It is important to recognize that the Weibull life distribution contains an underlying Poisson flaw distribution, which was described in the previous sub-section.

### C. LIFE CONVOLUTION

The intrinsic normalized life,  $\tau$ , for a given stress history,  $S(t)$ , is obtained by convoluting the effect of stress via the breakdown rule  $\kappa$ .

$$\tau \equiv \frac{1}{\hat{t}} \int_{t_i}^{t_f} \kappa(S(t)) dt ,$$

**Equation V-8**

where  $S(t)$  is a stress norm that is piecewise continuous in time  $t$ ,  $\hat{t}$  is a non-dimensionalizing and normalizing parameter for time,  $t_i$  is the initial time,  $t_f$  is the final time, and  $\kappa$  is a damage function. In the simplest case, this process reduces to the familiar Miner's Rule, which is a linear superposition of damage.

Different physical processes give rise to different forms of the damage function  $\kappa(S(t))$ . The power form and exponential form are explored. Combinations of the two forms are also possible.

### **1. Power Law Damage Function**

The first proposed damage function is defined using a power relation. This form has been observed to fit high cycle fatigue data in metals and is associated with flaw growth.

$$\kappa(S(t)) \equiv \left( \frac{S(t)}{C_1} \right)^b ,$$

**Equation V-9**

where  $b$  is a constant exponent, and  $C_1$  is a constant non-dimensionalizing parameter for stress. Both  $b$  and  $C_1$  are material constants. The constants are determined by fitting a line to Strength-Life data for a given material in log space where

$$b = \frac{1}{\text{slope}} ,$$

**Equation V-10**

and

$$C_1 = \exp(\text{intercept}).$$

**Equation V-11**

Substituting Equation V-9 into Equation V-8 yields,

$$\tau = \frac{1}{\hat{t}} \int_{t_i}^{t_f} \left( \frac{S(t)}{C_1} \right)^b dt,$$

**Equation V-12**

and substituting Equation V-12 into Equation V-6 yields,

$$\Xi(\tau) = \left( \frac{1}{\hat{t}} \int_{t_i}^{t_f} \left( \frac{S(t)}{C_1} \right)^b dt \right)^a.$$

**Equation V-13**

Finally, substituting Equation V-13 into Equation V-7 yields:

$$F(t|S) = 1 - \exp \left[ - \left( \frac{1}{\hat{t}} \int_{t_i}^{t_f} \left( \frac{S(t)}{C_1} \right)^b dt \right)^a \right].$$

**Equation V-14**

Next, the parameters from the life test are related to the parameters in standard Weibull form. Standard Weibull form is:

$$R(t) = 1 - F(t) = \exp \left[ - \left( \frac{t}{t_\beta} \right)^{\alpha_t} \right].$$

**Equation V-15**

So, Equation V-14 is rearranged and equated to Equation V-15.

$$\exp \left[ - \left( \frac{1}{\hat{t}} \int_{t_i}^{t_f} \left( \frac{S(t)}{C_1} \right)^b dt \right)^a \right] = \exp \left[ - \left( \frac{t}{t_\beta} \right)^{\alpha_i} \right]$$

**Equation V-16**

Every element in **Equation V-6** is now known.  $\hat{t}$  is an arbitrary normalizing parameter,  $C_1$ ,  $b$ ,  $t_\beta$ , and  $\alpha_i$  are determined from material testing, and  $a$  is the size effect parameter, which is unity if the test specimens are the same size as the actual part. Given a stress history, **Equation V-6** can be solved for life  $t$ .

## **2. Exponential Law Damage Function**

The second proposed damage function is defined using an exponential law. This form has been observed to fit low cycle fatigue data in metals and is associated with yielding.

$$\kappa(S(t)) \equiv \frac{1}{C_2} \exp \left( \frac{S(t)}{C_3} \right),$$

**Equation V-17**

where  $C_2$  is a constant, and  $C_3$  is a constant non-dimensionalizing parameter for stress.

Both  $C_2$  and  $C_3$  are material constants. The constants are determined by fitting a line to Strength-Life data for a given material in semi-log space where:

$$C_3 = \text{slope},$$

**Equation V-18**

and

$$C_2 = \exp(\text{intercept} / C_3),$$

**Equation V-19**

Substituting **Equation V-17** into **Equation V-8** yields:

$$\tau = \frac{1}{\hat{t}} \int_{t_i}^{t_f} \frac{1}{C_2} \exp \left( \frac{S(t)}{C_3} \right) dt,$$

**Equation V-20**

and substituting Equation V-20 into Equation V-6 yields:

$$\Xi(\tau) = \left( \frac{1}{\hat{t}} \int_{t_i}^{t_j} \frac{1}{C_2} \exp\left(\frac{S(t)}{C_3}\right) dt \right)^a.$$

**Equation V-21**

Substituting Equation V-21 into Equation V-7 yields:

$$F(t) = 1 - \exp \left[ - \left( \frac{1}{\hat{t}} \int_{t_i}^{t_j} \frac{1}{C_2} \exp\left(\frac{S(t)}{C_3}\right) dt \right)^a \right].$$

**Equation V-22**

Next, the parameters from the life test are related to the parameters in standard Weibull form.

So, Equation V-22 is equated to Equation V-15.

$$\exp \left[ - \left( \frac{1}{\hat{t}} \int_{t_i}^{t_j} \frac{1}{C_2} \exp\left(\frac{S(t)}{C_3}\right) dt \right)^a \right] = \exp \left[ - \left( \frac{t}{t_\beta} \right)^{a_i} \right].$$

**Equation V-23**

and the equation is solved for t.

### 3. Constant Stress Case Example

Having developed the above, the solution approach for the power law form of the damage function is to determine the parameters a, b, and C<sub>1</sub> from a known stress history. Once known, these parameters can be used to predict F(t) of another history.

For example, for a constant stress case defined as,

$$S(t) = \begin{cases} 0 & t < t_i \\ S_1 & t > t_i \end{cases},$$

**Equation V-24**

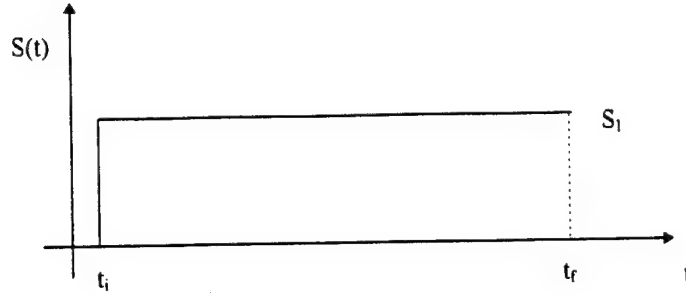


**Figure V-1**

$$\tau = \frac{1}{\hat{t}} \int_{t_i}^{t_f} \left( \frac{S_1}{C_1} \right)^b d\xi = \frac{1}{\hat{t}} \left( \frac{S_1}{C_1} \right)^b \int_{t_i}^{t_f} d\xi,$$

**Equation V-25**

or

$$\tau = \left( \frac{S_1}{C_1} \right)^b \frac{(t_f - t_i)}{\hat{t}}.$$

**Equation V-26**

Equation V-26 shows that life is proportional to elapsed time  $\left( \frac{t_f - t_i}{\hat{t}} \right)$  for a constant

load  $S_1$ . Since  $b$  is a negative number, an increase in  $S_1$  reduces life  $\tau$ .

Now, substituting into Equation V-13,

$$\Xi(\tau) = \left( \frac{S_1}{C_1} \right)^{ba} \left( \frac{t_f - t_i}{\hat{t}} \right)^a,$$

**Equation V-27**

and substituting Equation V-27 into Equation V-7,

$$F(t) = 1 - \exp \left[ - \left( \frac{S_1}{C_1} \right)^{ba} \left( \frac{t_f - t_i}{\hat{t}} \right)^a \right],$$

**Equation V-28**

which is the cumulative distribution function or cumulative probability of failure for the constant stress history.

Next, the parameters from the life test are related to the parameters in standard Weibull form. Equating Equation V-28 with Equation V-15,

$$\exp \left[ \left( \frac{S_1}{C_1} \right)^{ba} \left( \frac{t_f - t_i}{\hat{t}} \right)^a \right] = \exp \left[ - \left( \frac{t}{t_\beta} \right)^{\alpha_i} \right],$$

**Equation V-29**

and the equation is solved for t.

#### **4. Varying Stress Case Based on Rotor Kinematics**

The Tie Bar stress history is taken to be of the form:

$$S(\psi(t)) = S_m - S_a \cos(\psi(t) - 90^\circ),$$

**Equation V-30**

where

$$S_m = \frac{S_{\max} + S_{\min}}{2},$$

**Equation V-31**

$$S_a = \frac{S_{\max} - S_{\min}}{2},$$

**Equation V-32**



and  $\psi(t)$  is the rotor position in degrees. **Figure V-2** shows a typical stress history for the Tie Bar.

Substituting this new stress history into **Equation V-12**,

$$\tau = \frac{1}{t} \int_{t_0}^{t_f} [S_m - S_a \cos(\psi(\zeta) - 90^\circ)]^b d\zeta.$$

**Equation V-33**

Unlike the previous constant load case, the integrand in **Equation V-33** is not symbolically integrable. Therefore, the integral must either be solved numerically or approximated.

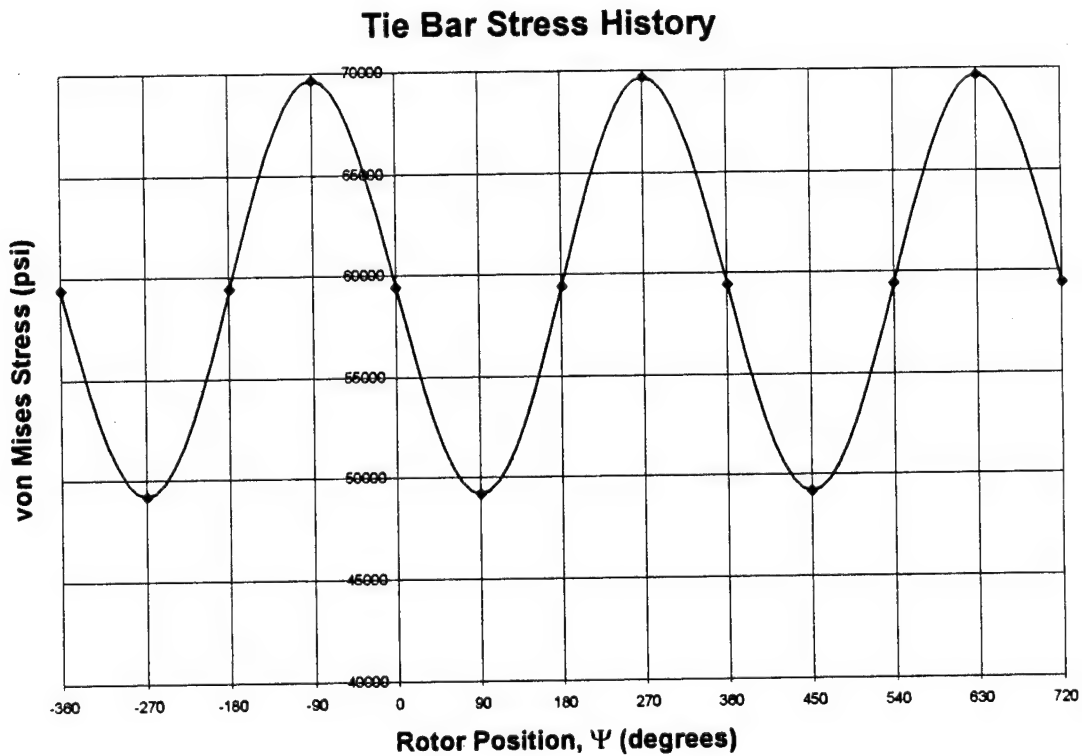


**Figure V-2** Typical Element Stress History

## VI. COUPON TESTS

Coupon tests were performed by the Tie Bar manufacturer to evaluate different manufacturing processes. The test coupons were single, modified production Tie-Bar straps. Each coupon had the center two components removed by machining.

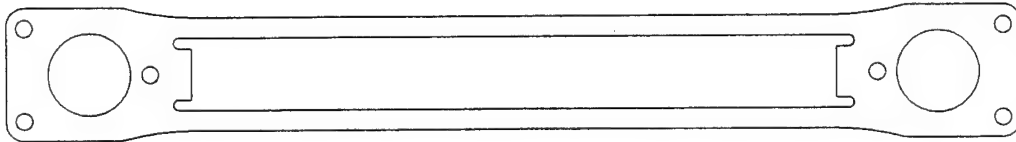


**Figure VI-1 Tie-Bar Coupon**

The following manufacturing process modifications were evaluated either individually or in combination:

- Stamping from new die
- Pre-twisting to 1800 micro-strain
- Production glass bead peening
- High intensity peening
- Peening at a 45 degree angle
- Chemical milling
- Deburring and steel shot peening

### **A. STAMPING FROM NEW DIE**

A new die was used to stamp some of the coupons to get a cleaner edge. The original die creates a sheared edge that is fairly rough and is thought to provide numerous crack-initiation sites.

### **B. PRE-TWISTING TO 1800 MICRO-STRAIN**

Control system checkouts are performed on the ground with the rotors stationary. These control checks twist the Tie-Bar approximately 22.5°. Some bending also occurs due to the rotor

blade weight. A strain-gaged Tie-Bar installed on an aircraft showed a maximum compression strain of -1800 micro-inches during this control check.

To emulate this check, some coupons (two at a time) were put in a twist test fixture with a spacer between them so they would experience the same loading as the outermost straps of an entire Tie-Bar assembly. The coupons were twisted to -1800 micro-inches as read from a strain gage mounted on the outer strap near a slot end. The coupons were then removed from the twist fixture and tested in simple tension-tension until failure.

### **C. 6° TWIST LOAD**

Some specimens were subjected to an added load calculated by twisting the coupon 6°. Each coupon was not actually twisted. Instead, a strain gage was mounted on a coupon at the slot radius and the coupon was mounted in the twist test jig. The coupon was twisted 6° and the strain was measured. This strain was converted to stress. The additional coupon load was calculated assuming this stress equated to a nominal (P/A) stress. The coupon was then subjected to this twist load plus the standard fatigue load.

The coupons were tested in a tension-tension fatigue machine with a sinusoidal loading. The load blocks were repeated until 500 blocks were complete or the coupon failed, except as noted. The coupon load blocks are listed in the appendix **Table VIII-1**. A table of the various configurations and their associated lives are also located in the appendix **Table VIII-2**.

### **D. DETERMINING MATERIAL PARAMETERS**

The coupon geometry was modeled using two finite-element models: one for the standard coupons, and one for the chemically milled coupons. The chemically milled coupons had 0.002 inches of material removed from each surface, and the second finite element model reflects this. The basic load case for the models was a 0.1 inch displacement on each end of the coupon to put the coupon in tension.

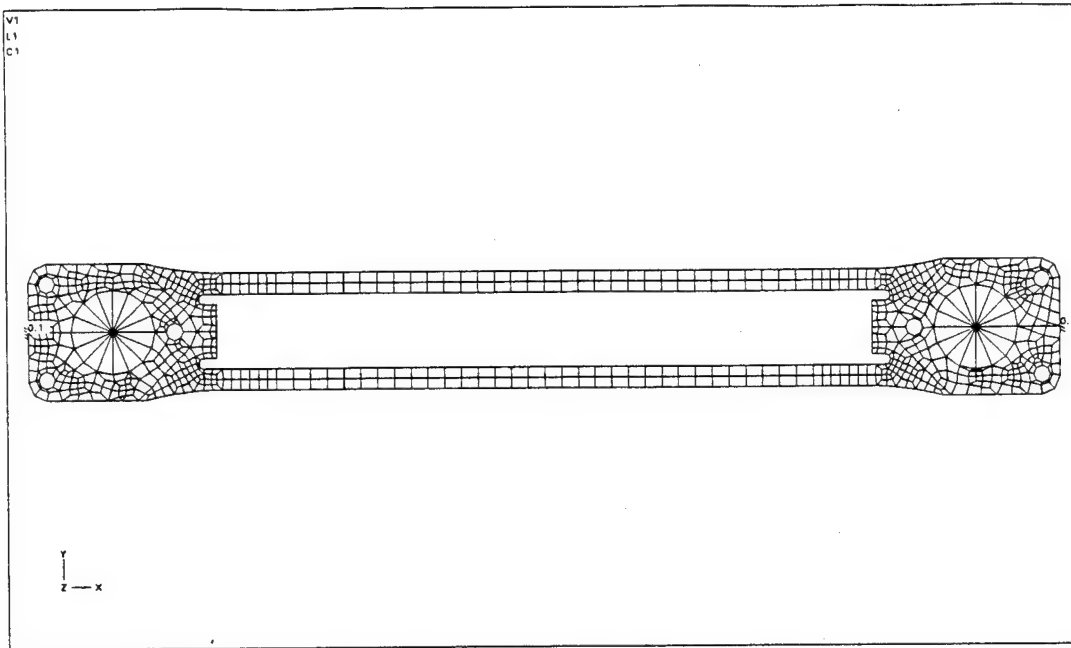


**Figure VI-2 Coupon Finite Element Model**

The T1 Constraint Force was calculated for each model and was scaled for each coupon test Load Profile. These scale factors were applied to the finite element models to recreate the coupon load conditions. Maximum coupon von Mises stresses were recorded for each Load Profile. These maximum von Mises stresses were converted to alternating stresses,  $S$ , using the Goodman relation.

$$\frac{\sigma_a}{S_n} + \frac{\sigma_m}{S_u} = 1,$$

**Equation VI-1**

where  $S_n$  is the fully reversed stress level corresponding to the same life as that obtained with the stress conditions,  $\sigma_a$  and  $\sigma_m$ , and  $\sigma_a$  and  $\sigma_m$  are the von Mises stress amplitude and mean stress determined from the finite element model. The results are tabulated in the appendix and are plotted in **Figures V-3 to V-10**. These figures have been fitted with lines using a least squares method. In the least squares method, each data point is equally weighted and is an expedient method of determining the central tendency of the fatigue behavior, i.e. the mean of the S-N curve.

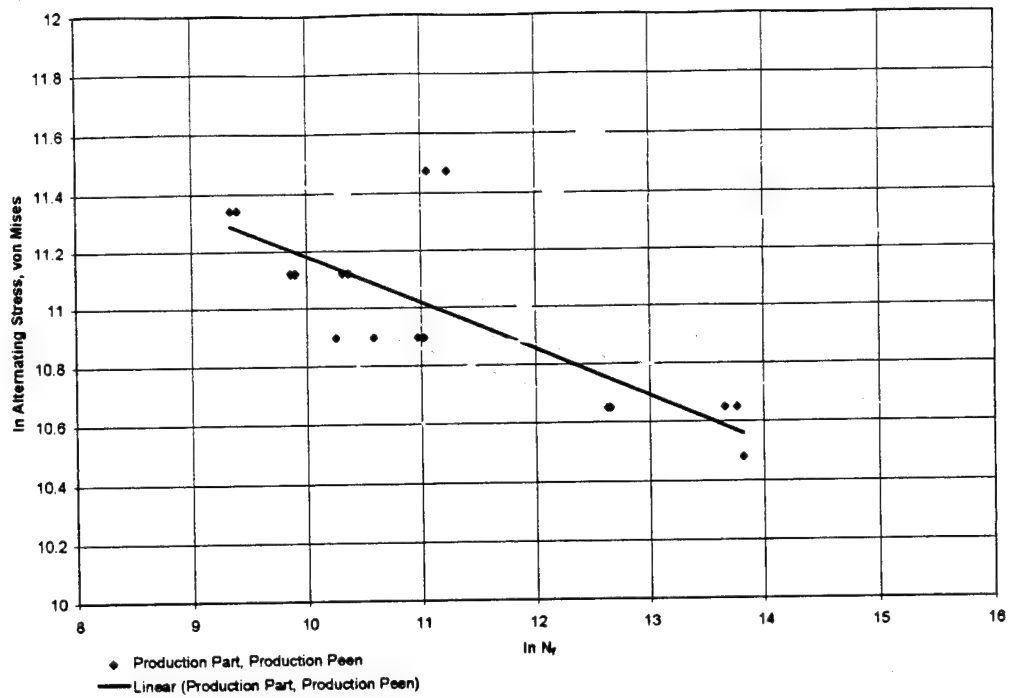


**Figure VI-3 Log-Log S-n Plot of Coupon Test Data, Production Part and Peen**

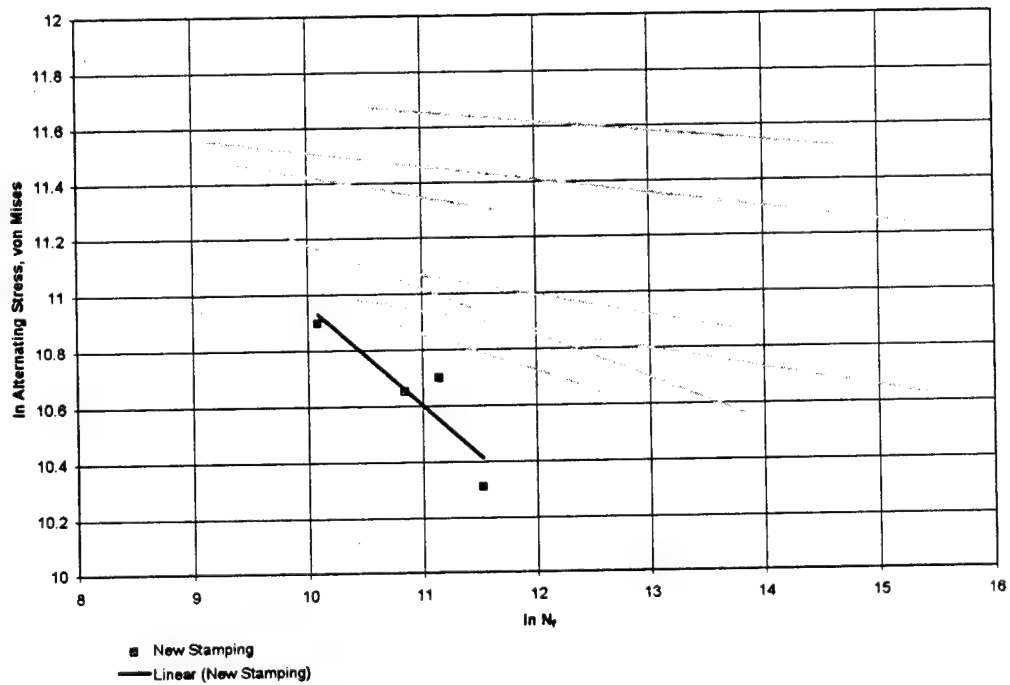


**Figure VI-4 Log-Log S-n Plot of Coupon Test Data, New Stamping**

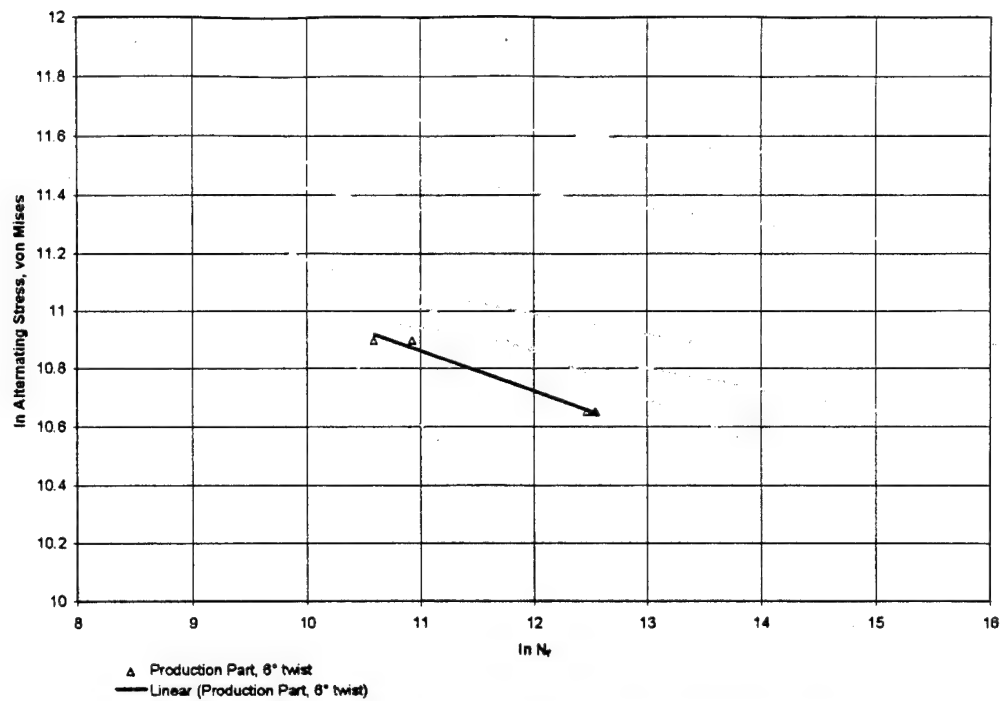


**Figure VI-5 Log-Log S-n Plot of Coupon Test Data, Production Part, 6° Twist**

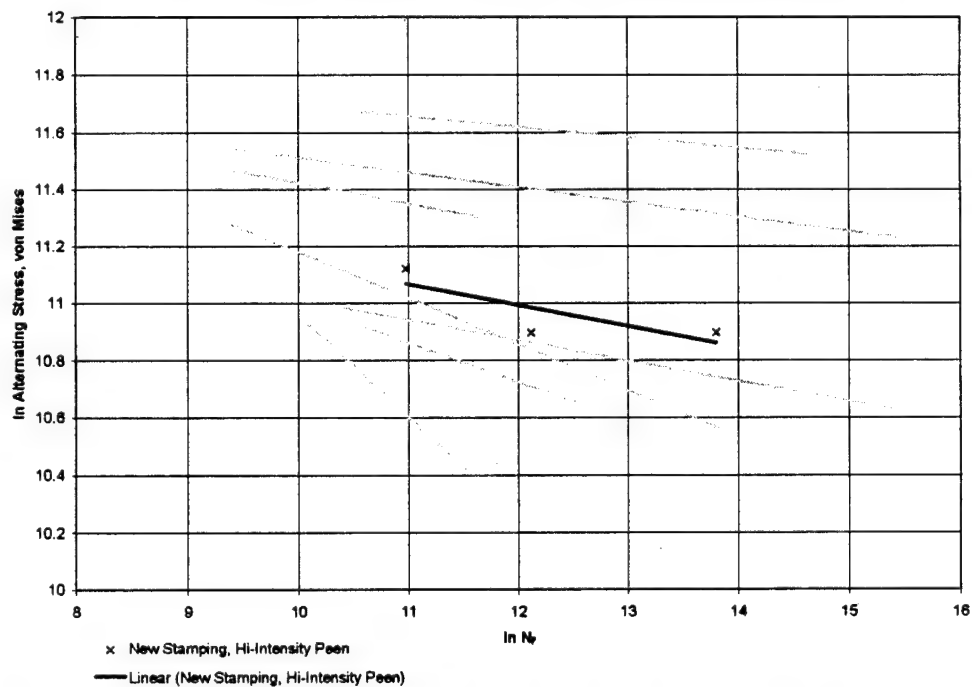


**Figure VI-6 Log-Log S-n Plot of Coupon Test Data, New Stamping, Hi-Intensity Peen**

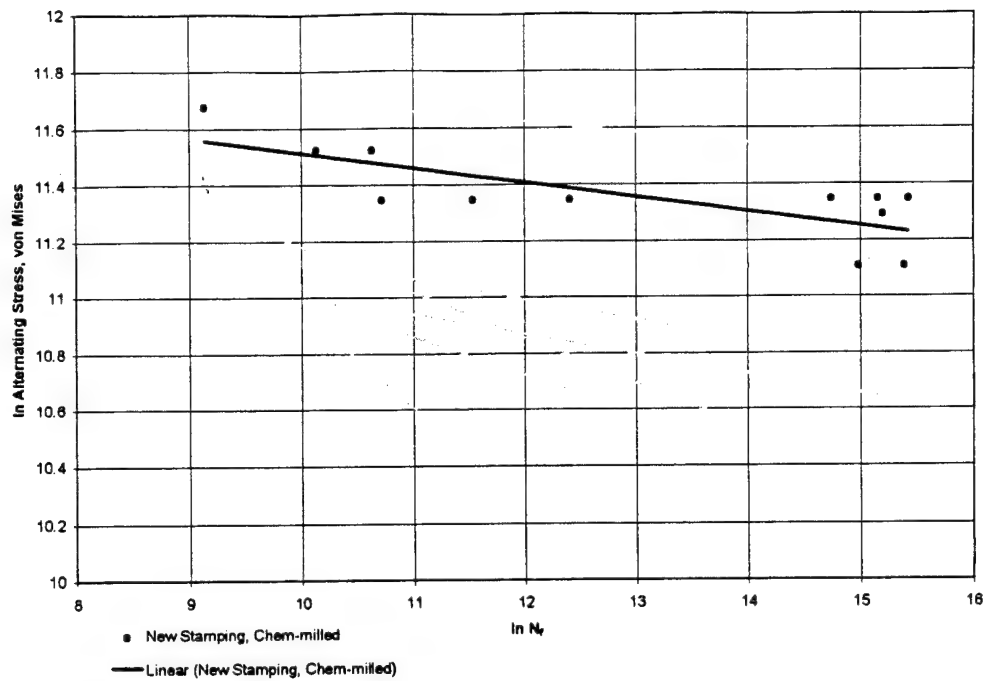


**Figure VI-7 Log-Log S-n Plot of Coupon Test Data, New Stamping, Chem-Milled**

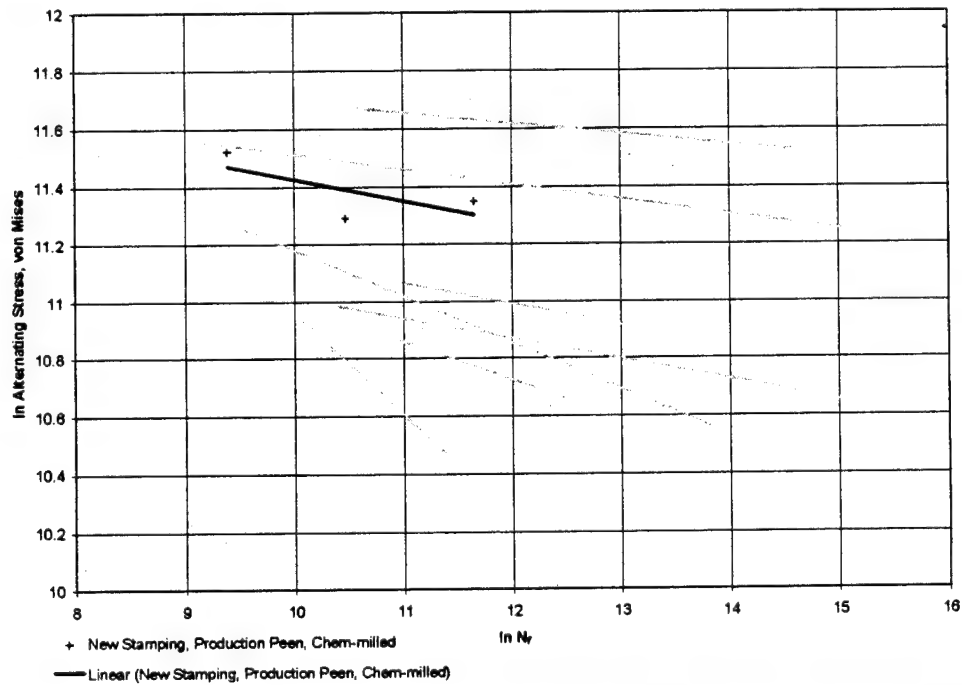


**Figure VI-8 Log-Log S-n Plot of Coupon Test Data, New Stamping, Production Peen, Chem-Milled**

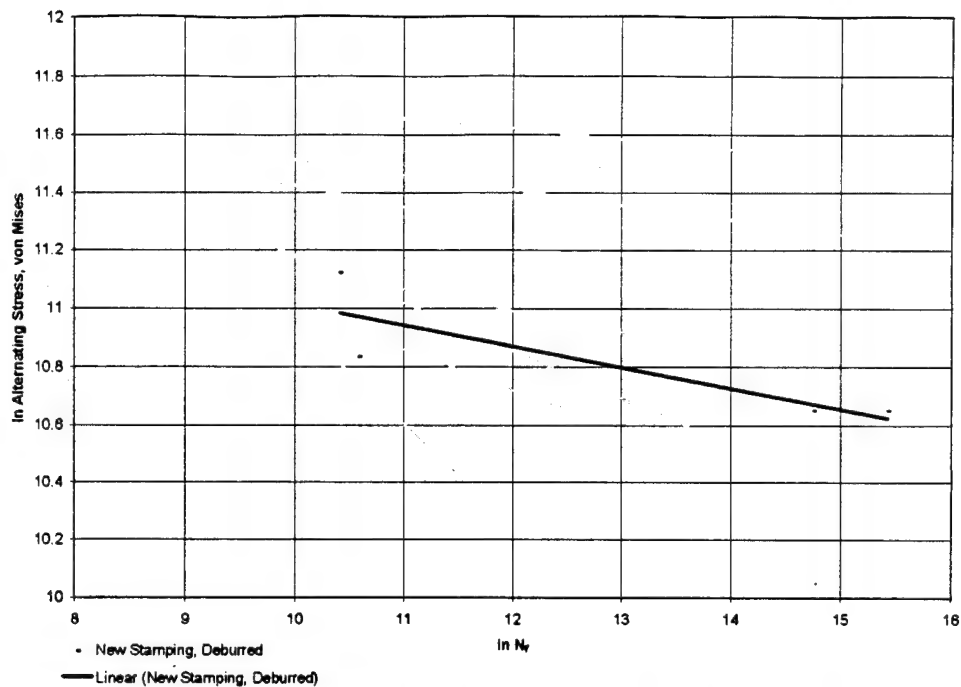


**Figure VI-9 Log-Log S-n Plot of Coupon Test Data, New Stamping, Deburred**

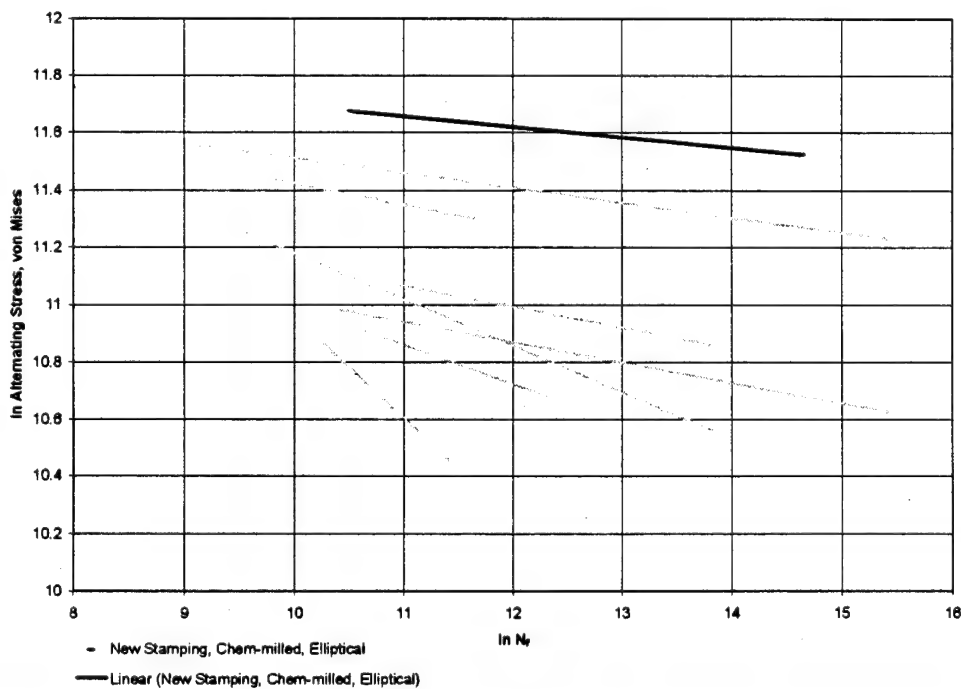


**Figure VI-10 Log-Log S-n Plot of Coupon Test Data, New Stamping, Chem-Milled, Elliptical Slot**



For each alternating stress level in **Figures V-3 to V-10**, there are several values of life. There is a mean distribution for each of these stress levels. The fitted lines can be interpreted as the mean life of the population at each stress level and may be corrected to the location parameter by the relation

$$\mu = \beta \cdot \Gamma\left(1 + \frac{1}{\alpha}\right).$$

#### Equation VI-2

For this conversion, the shape parameter  $\alpha$  must be known. To estimate  $\alpha$ , a maximum likelihood estimator technique can be used to find the parameters of a Weibull distribution that fits the data at each stress level. Such extensive data interpretation has not been pursued in the investigation. Instead, it was assumed that the strength-life relation is homologous; that is, the fractional life S-N curves do not criss-cross. Under this assumption, the shape parameter for strength  $\alpha_\sigma$  can be related to the shape parameter for life  $\alpha_t$  by

$$\alpha_t = \frac{b}{\alpha_\sigma},$$

#### Equation VI-3

where  $b$  has already been determined by the least squares fit. Typically, strength data are more plentiful and the coefficient of variability  $cv_\sigma$  in strength are reported in open literature to be 0.5%. The coefficient of variation can be converted to the shape parameter by the approximation

$$\alpha_\sigma \cong \frac{1.2}{cv_\sigma}.$$

#### Equation VI-4

**Table VI-1** tabulates the material parameters for the power law development in the previous section. Larger values of  $b$  indicate longer life.

Condition	b	C <sub>1</sub> (psi)
Production Part, Production Peen	-6.16	364,171
New Stamping	-2.77	2,121,151
Production Part, 6° Twist	-7.26	237,081
New Stamping, Hi-intensity Peen	-13.61	143,599
New Stamping, Chem-milled	-19.23	168,054
New Stamping, Production Peen, Chem-milled	-13.21	195,128
New Stamping, Deburred	-14.03	123,731
New Stamping, Chem-milled, Elliptical	-27.36	172,509

**Table VI-1      Coupon Test Calculated Parameters**



## VII. CONCLUSIONS

This research developed a probability modeling method that can aid the prediction of a Tie Bar design to meet desired life and reliability levels. The model allows the effects of changes in geometry, material, and manufacturing processes to be quantified. Since the model can predict life, it could be used for the current Tie Bar to help determine a safe time interval between inspections.

Two design concepts were explored in this investigation. The elliptical slot design did not reduce stress concentration in all flight kinematic configurations. Whether the elliptical slot design will yield longer life, is not definitive. The reduced constraint design proposed herein provided much more stress concentration reduction as suggested by the finite element study. This reduced constraint design may produce large gains in life over the current design.



## VIII. RECOMMENDATIONS

Some field data has been recorded on current-design Tie Bars. It is recommended that detailed breakage data including part hours, number of broken components, and location of broken components continue to be recorded. This data can be used to calibrate the model created in this investigation.

While the modeling method developed is basically complete and parts of it have been used to calculate results, more effort needs to be spent on organizing the NASTRAN output and feeding it through the convolution and probability models. The coupon data could be analyzed more thoroughly to provide better material parameters. This investigation only focused on one strap (4 components) of a two-strap model. Further work should be done to predict the probability of failure of at least the eight components of the two outer straps.

Boeing Vertol is qualifying new designs for the Tie Bar through testing. Results of this testing need to be compared to the model results to ensure the model's validity. Field data can be compared to both the model results and the testing results to determine what further load and life modeling needs to be done.

Better automation and generalization of the methods described in this investigation would be quite useful. A finite element post-processor could theoretically be developed to study the Tie Bar as well as any general structure.



## APPENDIX

Load Profile	Mean Load (lbs)	Load Amplitude (lbs)	Minimum Load (lbs)	Maximum Load (lbs)	Block Cycles	Alternating Stress (psi)
A	1406	940	466	2346	10,000	84,438
	1109.5	1109.5	0	2219	10	87,411
B	1406	752	654	2158	10,000	67,550
	1109.5	1109.5	0	2219	10	87,411
C	1406	470	936	1876	10,000	42,219
	1109.5	1109.5	0	2219	10	87,411
D	1406	470	936	1876	10,000	42,219
	1481	1481	0	2962	10	137,926
	2633	329	2304	2962	132*	70,382
E <sup>1</sup>	1011	470	541	1481	10,000	35,576
	1109.5	1109.5	0	2219	10	87,411
F	950	600	350	1550	1,000,000	44,338
G <sup>1</sup>	1406	752	654	2158	10,000	67,550
	1481	1481	0	2962	10	137,926
	2633	329	2304	2962	132*	70,382
H	1406	601	805	2007	10,000	53,987
	1109.5	1109.5	0	2219	10	87,411
I	1406	601	805	2007	10,000	53,987
	1481	1481	0	2962	10	137,926
	2633	329	2304	2962	132*	70,382
J <sup>1</sup>	570	466	104	1036	1,000,000	30,002
K	1220	847	373	2067	10,000	69,935
	961.5	961.5	0	1923	10	71,371
L	1220	847	373	2067	10,000	69,935
	961.5	961.5	0	1923	10	71,371
M	1220	1010	210	2230	10,000	83,393
	961.5	961.5	0	1923	10	71,371
N	1220	1174	46	2394	10,000	96,934
	961.5	961.5	0	1923	10	71,371
O	1220	800	420	2020	10,000	66,054
	961.5	961.5	0	1923	10	71,371
P <sup>2</sup>	2830	350	2480	3180	10,000,000	96,216
Q <sup>2</sup>	2830	433	2397	3263	10,000,000	119,033
R	1406	564	842	1970	10,000	50,663
	1109.5	1109.5	0	2219	10	87,411

\* Applied One Time Every Five Blocks

<sup>1</sup> 1,000,000 cycles

<sup>2</sup> 10,000,000 cycles

Alternating Stress is calculated using a Goodman relationship and von Mises stress from the coupon finite element model.

**Table VIII-1 Coupon Load Conditions**



Specimen ID	Production Part	New Stamping	6° Twist	Production Peen	High-Intensity Peen	45° Peen	Chem-milled	Deburred	Elliptical	Load Profile	Life (cycles)
1	X			X						A	12,000
1B	X			X						P	75,000
2B	X			X						P	63,000
2	X			X						A	11,300
3	X			X						B	19,000
4	X			X						B	19,800
5	X			X						C	313,000
6	X			X						C	305,000
7	X			X						D	950,000
8	X			X						D	852,000
9	X			X						E	1,000,000
10	X			X						E	1,000,000
11	X			X						G	31,480
12	X			X						G	29,900
13	X			X						H	39,256
14	X			X						I	58,000
15	X			X						H	28,200
16	X			X						I	61,000
17		X								F	69,000
18		X								J	101,000
19		X								C	51,000
20		X								H	24,000
21	X		X							H	39,700
22	X		X							H	55,400
23	X		X							C	259,700
24	X		X							C	281,000
25		X			X					B	58,100
26		X			X					H	183,000
27		X			X					H	980,000
28						X				H	61,800
29						X				H	58,000
30		X					X			K	3,800,000
30		X					X			L	244,000
31		X					X			H	3,200,000
34		X					X			H	4,800,000
34		X					X			K	2,520,000
34		X					X			L	45,000
35		X					X			L	102,000
36		X					X			M	25,000
37		X					X			N	9,257
38		X		X			X			M	11,900
39		X		X			X			L	114,500
40		X		X			X			O	35,000
41		X					X			O	3,970,000
42		X					X			M	41,100
43		X					X			L	5,000,000
44		X						X		B	33,100

Specimen ID	Production Part	New Stamping	6° Twist	Production Peen	High-Intensity Peen	45° Peen	Chem-milled	Deburred	Elliptical	Load Profile	Life (cycles)
45		X						X		R	39,250
46		X						X		C	2,550,000
47		X						X		C	5,000,000
48		X					X		X	M	2,270,000
49		X					X		X	N	37,000

**Table VIII-2 Coupon Test Summary**



## **LIST OF REFERENCES**

1. O'Connor, J. O., "Probabilistic Reliability Modeling of Fatigue on the H-46 Tie Bar," Master's Thesis, Naval Postgraduate School, September 1994.



## BIBLIOGRAPHY

Allen, D. H., Haisler, W. E., *Introduction to Aerospace Structural Analysis*, John Wiley & Sons, Inc., 1985.

Bannintine, J. A., Comer, J. J., and Handrock, J. L., *Fundamentals of Metal Fatigue Analysis*, Prentice-Hall, Inc., 1990.

Lewis, E. E., *Introduction to Reliability Engineering*, John Wiley & Sons, Inc., 1986.

Phoenix, S. L., and Wu, E. M., "Statistics for the Time Dependent Failure of Kevlar-49 Composites: Micromechanical Modeling and Data Interpretation," paper presented at the IUTAM Symposium on Mechanics of Composite Materials, Virginia Polytechnic Institute and State University, Blacksburg, Virginia, 16-19 August 1982.

Prouty, R. W., *Helicopter Performance, Stability, and Control*, Prindle, Weber, & Schmidt, 1986.

Sikorsky Aircraft Company, *Parametric Investigation of the Aerodynamic and Aeroelastic Characteristics of Articulated and Rigid (hingeless) Helicopter Rotor Systems*, U. S. Army Transportation Research Command technical report 64-15, 1964.



## INITIAL DISTRIBUTION LIST

1. Defense Technical Information Center ..... 2  
     Cameron Station  
     Alexandria, Virginia 22304-6145
  
2. Library, Code 52 ..... 2  
     Naval Postgraduate School  
     Monterey, California 93943-5101
  
3. Director, Naval Air Systems Command DET ..... 3  
     Program Manager Air (Field) - 226  
     Mr. Jon Winchester  
     PSC Box 8026  
     Cherry Point, North Carolina 28533-0026
  
4. Department of the Navy ..... 1  
     Naval Air Systems Command  
     Attention: AIR 530A  
     1421 Jefferson Davis Highway  
     Arlington, Virginia 22243-5300
  
5. Prof. Daniel J. Collins, Code AA/Co ..... 1  
     Chairman  
     Department of Aeronautical Engineering  
     Naval Postgraduate School  
     Monterey, CA 93943-5000
  
6. Prof. Edward M. Wu, Code AA/Wu ..... 4  
     Department of Aeronautical Engineering  
     Naval Postgraduate School  
     Monterey, CA 93943-5000
  
7. Dr. Donald Danielson, Code MA/Dd ..... 1  
     Department of Mathematics  
     Naval Postgraduate School  
     Monterey, California 93943-5101
  
8. Mr. George J. Schneider ..... 1  
     Sikorsky Aircraft  
     6900 Main Street  
     Mail Stop S314A2  
     Stratford, Connecticut 06497
  
9. AIRINC Research ..... 1  
     Attention: Tim Ryan  
     2551 Riva Road  
     Annapolis, Maryland 21401



10. LT Greg Sauter ..... 1  
936 Summerside Ct.  
Virginia Beach, VA 23456